Impact of cysteine 106 oxidation on function and localisation of the Parkinson's disease-related protein DJ-1

by

Helena Amalie Hushagen

Thesis submitted in partial fulfilment of the requirements

for the degree of Master of Science

Department of Biological Sciences

University of Bergen

June 2019

Acknowledgements

First of all, I would like to thank my main supervisor, Kari Fladmark, for letting me work on such an interesting project. It has been a great opportunity to try a broad range of different techniques. Being enthusiastic about my work. You have believed in my abilities, been enthusiastic about my results and had the patience to let me figure things out at my own pace to work more independently. I am especially thankful for the excellent and fast feedback on the writing and for the opportunity to be included in the ongoing projects in the lab.

Thank you to my co-supervisor, Amanda Edson, for sharing your office, your knowledge and for supporting me throughout my entire project. You have been a daily dose of positivity, always encouraging me even when things didn't go as planned.

Thank you to Ann Kristin Frøyset, my unofficial supervisor, for all the practical guidance in the lab, for answering my many questions and for always keeping your office door open.

Thank you to my fellow students at the CellStress lab for creating such a friendly and helpful work environment in such a short time. Although our time together was short, it was really nice to get some life back around the lab benches.

I would also like to thank everyone at the department who have helped me, answered questions, lent me reagents in a pinch or just asked me how I was doing. It has been a great environment.

Finally, I would like to thank my family and friends for their support during these last few months, and to Alexander for being a wonderfully understanding and supporting partner through all of this.

Table of contents

Publications

During the work on my master I have contributed to the following work:

Edson, A.J., **Hushagen, H.A.**, Frøyset, AK., Khan, E., Di Stefano, A., Fladmark, K.E. (2019): "Dysregulation in the brain protein profile of zebrafish lacking the Parkinson's disease related protein DJ-1", <u>Molecular Neurobiology.</u> (accepted May 2019)

Edson, A. J., **Hushagen, H.A.**, Fladmark, K.E. (2019): "DJ-1 in astrocytic neuroprotection to oxidative stress", in <u>Oxidative Stress and Dietary Antioxidants in Neurological Diseases.</u> Academic Press. (accepted April 2019)

Selected abbreviations

Abbreviation	Full length word
ASK1	Apoptotic signal regulating kinase 1
DAB	Diaminobenzidine
Dpf	Days post fertilization
eGFP	Enhanced green fluorescent protein
ER	Endoplasmic reticulum
GFP	Green fluorescent protein
GSH	Glutathione
HRP	Horse radish peroxidase
Hpf	Hours post fertilization
iNOS	Inducible nitric oxide synthase
KO	Knockout
MAM	Mitochondria-associated ER membranes
MIM	Mitochondrial inner membrane
Nrf2	Nuclear factor erythroid 2-related factor 2
OMM	Outer mitochondrial membrane
O/N	Over night
ORF	Open reading frame
PD	Parkinson's disease
RNS	Reactive nitrogen species
ROS	Reactive oxygen species
SDS-PAGE	Sodium dodecyl sulphate polyacrylamide gel electrophoresis
SN	*Substantia nigra*
TEM	Transmission electron microscopy
TH	Tyrosine hydroxylase
U	Enzymatic Unit
WT	Wild type

Abstract

DJ-1 is a multifunctional ubiquitously expressed protein encoded by the PARK7 gene in humans. Dysfunction of DJ-1 is implicated in various human diseases, particularly neurodegenerative diseases such as Parkinson's disease (PD) and Alzheimer's disease (AD). The highly conserved cysteine residue at position 106 has been shown to be an important site for posttranslational modifications modulating the activity and localization of DJ-1, and acting as a sensor of oxidative and nitrosative stress in the cell. The potential neuroprotective role of astroglial DJ-1 as a regulator of antioxidant gene expression and as an antioxidant itself has been demonstrated *in vitro* and in multiple animal models exposed to oxidative stressors. To further our understanding of DJ-1's protective role in astroglia and the importance of the conserved C106, we developed a mutant zebrafish line with astroglia-restricted expression of DJ-1$_{C106A}$ driven by the promotor region of the glial fibrillary acidic protein (GFAP) (*park7$^{-/-}$,Tg(gfap:egfp-2A-flag-zDJ-1$_{C106A}$)*) (UiB2003). The response of UiB2003 larvae to the PD phenotype-inducing mitochondrial complex I inhibitor rotenone was compared to that of wild type, DJ-1 knockout (DJ-1 KO) and a corresponding astroglial-restricted DJ-1$_{WT}$-expressing zebrafish line (*park7$^{-/-}$,Tg(gfap:egfp-2A-flag-zDJ-1)*) (UiB2001). Both UiB2003 and UiB2001 larvae displayed a drastically lower survival than WT and DJ-1 KO, as well as lowered heart rate compared to controls. The UiB2003 larvae also showed significantly higher incidence of edema than DJ-1 KOs. The expression of tyrosine hydroxylase (TH), a marker for dopaminergic cell death, was reduced in UiB2003 larvae compared to WT under basal conditions. The line did however sow a lower induction of inducible nitric oxide synthase (iNOS), a marker for intracellular stress, than DJ-1 KO larvae where marker was significantly increased. Adult UiB2003 fish showed a reduced complex I activity in skeletal muscle compared to WT fish, while the activity in the astroglia-rich brain was unaffected, indicating C106 independent effect of DJ-1 on complex I regulation.

In order to examine the role of cysteine 106 on the ultrastructural localization of DJ-1 in response to oxidative stress, fusion proteins of DJ-1$_{WT}$/DJ-1$_{C106A}$ and the peroxidase APEX2 were used to facilitate the targeted diaminobenzidine-staining of the SH-SY5Y neuroblastoma cells following treatment with rotenone. This produced a DJ-1 specific staining pattern that could be visualized by transmission electron microscopy and revealed a mainly cytosolic expression of DJ-1, with no staining in the mitochondrial interior, possibly with some faint expression at the outer mitochondrial membrane. Additionally, the overexpression of the DJ-1$_{WT}$/DJ-1 induced increased contact between the endoplasmic reticulum (ER) and mitochondria

compared to non-transfected cells. Both the localization pattern and induced ER-mitochondria contact was independent of the C106 and of rotenone-induced oxidative stress.

In conclusion, the astroglia-restricted expression of DJ-1$_{C106A}$, does not protect zebrafish larvae from rotenone-induced oxidative insult and even displays a negative effect under baseline conditions. On the contrary, it appears to facilitate a stronger negative response and heightened sensitivity to the toxicant. On the other hand, DJ-1$_{C106A}$ retains its ability to regulate complex I in adult fish and iNOS in larvae. The C106 mutation does not affect the intracellular localization of DJ-1 nor the ability of DJ-1 overexpression to induce ER-mitochondria association.

1 Introduction

1.1 Parkinson's disease

Parkinson's disease (PD) is among the most common neurodegenerative human diseases, afflicting around 1% of people above age 60 (de Lau and Breteler, 2006). It is a progressive disorder clinically characterised by tremors, bradykinesia (slowed movement) and postural instability. The hallmark of PD is the loss of dopaminergic neurons in the *substantia nigra* (SN) of the mid brain, leading to reduced dopamine levels in the *striatum*, and the formation of abnormal protein aggregates in the neurons known as Lewy bodies (Twelves et al., 2003). The ethology and pathogenesis of PD is not fully understood, however oxidative stress, protein aggregation and mitochondrial dysfunction is thought to play a major role (Greenamyre and Hastings, 2004).

PD manifests as two distinct forms: sporadic and familial. While the familial form accounts only for about 10% of disease cases, the majority of advances made in understanding the underlying mechanism of PD and elucidating the pathways and proteins involved have been achieved by studying this form. Some notable genes found to lead to PD when mutated are park7, α-synuclein, parkin, PTEN-induced punitive kinase 1 (PINK1) and ubiquitin carboxyl-terminal hydrolase isozyme L1 (UCHL-1) (Bonifati et al., 2003, Dawson and Dawson, 2003). The same gene products are believed to be involved in the pathogenesis of sporadic forms of PD, dysregulated due to environmental effects.

Loss of function mutations in the *Park7* gene encoding DJ-1 has been linked to autosomal recessive early-onset Parkinson's disease (Bonifati et al., 2003). The involvement of DJ-1 in the initial stress response of PD is supported by elevated levels of DJ-1 found in the brains of PD patients, particularly in the astrocytes (Bandopadhyay et al., 2004), as well as increased levels of DJ-1 in other neurodegenerative disorders such as Alzheimer's disease, Pick's disease, progressive supranuclear palsy and multiple sclerosis (Neumann et al., 2004, van Horssen et al., 2010). Furthermore, DJ-1 has been found to be highly oxidatively modified in post mortem samples of PD patients and to colocalize with pathogenic tau inclusions in multiple neurodegenerative disorders (Choi et al., 2006, Neumann et al., 2004, Kumaran et al., 2007).

1.2.1 The DJ-1 protein

DJ-1 is a small (189 amino acids) protein deglycase encoded by the *PARK7* gene. The protein is ubiquitously expressed and highly conserved (Bonifati et al., 2003). DJ-1 adopts a helix-strand-helix sandwich structure and has been found to form a homodimer based on crystallographic studies (Honbou et al., 2003, Wilson et al., 2003). Of particular interest in this regard is the discovery of a loss-of-function mutant variant of DJ-1 where a highly conserved alpha-helical leucine residue is substituted for a proline. This L166P mutant has been found to cause a hereditary form of PD (Bonifati et al., 2003). Following this discovery other PD causative mutations such as M26I, L10P, and P158Δ have also been found to impair dimerization *in vitro* (Repici et al., 2013). The inability to dimerize is thought to be the direct cause of dysfunction, making dimerization crucial for the activity of DJ-1.

DJ-1is found mainly in the cytoplasm under basal conditions, with a small pool inhabiting the nucleus and associated with the mitochondria. It has been suggested that the mitochondrial and nucleic localization of DJ-1 can change upon oxidative insult leading to stepwise translocation into the mitochondria and then the nucleus (Junn et al., 2009). Conversely, one study based on subcellular fractionation found DJ-1 to localize to the mitochondria in untreated SH-SY5Y cells (Zhang et al., 2018). Others have found mitochondrial localization to be dependent on oxidative stressors (Canet-Aviles et al., 2004, Junn et al., 2009) or a result of nutrient deprivation (Cali et al., 2015). There are also conflicting results for the sub-mitochondrial localization of DJ-1. Outer membrane-only, inter membrane space and matrix-restricted or matrix has been proposed (Canet-Aviles et al., 2004, Junn et al., 2009, Cali et al., 2015).
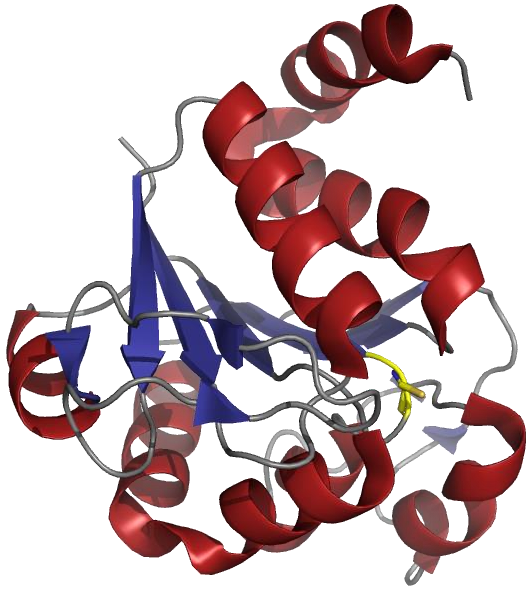
Fig. 1.1 Human DJ-1 monomer. Cartoon representation of the human DJ-1 monomer with α-helices shown in red, β-strands in blue and loops in grey. The cysteine at position 106 is shown in yellow and can be seen in the active seat of the protein.

1.2.2 The many functions of DJ-1

DJ-1 is a multifunctional protein and has over the years been found involved in a myriad of different pathways and cellular functions. It was first discovered by Nagakubo et al. as a novel oncogene product able to transform mouse NIH3T3 cells in a *ras*-dependent manner (Nagakubo et al., 1997). As a protein and nucleotide deglycase, DJ-1 acts in countering the spontaneous glycation of macromolecules in the cell. Proteins that are non-enzymatically deactivated by the addition of methylglyoxal and glyoxal to cysteine, arginine, and lysine residues, can be returned to their functional state by DJ-1-mediated repair (Richarme et al., 2015). DJ-1 is also involved in the regulation of multiple pathways in signal transduction. Among these are positive regulation of proliferation and survival via activation of the phosphatidylinositol-3-kinase (PI3K)/Akt pathway and extracellular signal-regulated kinase (ERK1/2) pathway. It acts anti-apoptotic through inhibition of apoptosis signal regulating kinase 1 (ASK1) as well as mitogen-activated protein kinase kinase kinase 1 (MAP3K1), both parts of the apoptosis signalling cascade (Oh and Mouradian, 2017). Another function is in male fertility. A DJ-1 homolog in rat, CAP1, was found to decrease in sperm corelating with decreasing fertility, while DJ-1 double knockout (KO) in Drosophila lead to male infertility (Wagenfeld et al., 1998, Hao et al.,

2010). Additionally, DJ-1 has been found to act as a positive regulator of the androgen receptor (AR) by binding to the AR-binding transcriptional regulator PIASxα (Takahashi et al., 2001).

Many of the DJ-1 activities relate to defence against oxidative stress. In addition to acting as an antioxidant in itself, scavenging H_2O_2 by oxidation of cysteine 106, DJ-1 is able to induce expression of antioxidant genes of the glutathione and thioredoxin pathways (Andres-Mateos et al., 2007, Raninga et al., 2017). Nuclear factor erythroid 2-related factor 2 (Nrf2) has an overarching role in the regulation of these genes through the Nrf2/ARE pathway and DJ-1 has been shown to act upstream of this regulator (Clements et al., 2006). Furthermore, DJ-1 acts as a chaperone on α-synuclein, the main component of Lewy bodies, preventing aggregation (Shendelman et al., 2004). DJ-1 is also involved in protein turnover and has been found to regulate the 20s proteasome (Moscovitz et al., 2015). DJ-1 is central in maintaining the correct morphology and function of mitochondria, additionally affecting autophagy of dysfunctional mitochondria, as shown by loss of DJ-1 leading to dysregulation of these activities (Krebiehl et al., 2010). In the context of PD and this thesis, DJ-1's role in the defence against oxidative stress, maintenance of mitochondrial function and overall neuroprotection will be in focus.

1.2.3 Post-translational modifications regulate the functions of DJ-1

DJ-1 is subject to a variety of posttranslational modifications, notably oxidation, SUMOylation, phosphorylation, nitrosylation and gluthationylation (Ariga et al., 2013, Raninga et al., 2017). These have different roles in the many functions of DJ-1. SUMO-1 conjugation at lysine 130 has been shown to be important for DJ-1 mediated cell growth, anti-apoptosis activity in UV-induced apoptosis but also for *ras*-dependent transformation, with K130 mutation abrogating these functions (Shinbo et al., 2006). DJ-1 has also been found to be subject to p53-dependent phosphorylation. The functional role of DJ-1 phosphorylation is largely unknown, but it has been suggested that it may play a role in regulating the anti-apoptotic functions of the protein (Rahman-Roblick et al., 2008). Glutahionylation of DJ-1 at C53 and C106 has been shown to be involved in targeting DJ-1 for degradation *in vitro* and *in vivo* (Johnson et al., 2016). This is further supported by the observation that loss of glutaredoxin1, the main deglutathionylating enzyme in cells, leads to loss of DJ-1 (Saeed et al., 2010).

Oxidation is thought to be the central player in DJ-1 activity modulation. DJ-1 has been found to adopt multiple oxidation states resulting in a pI shift that can be observed by two-dimensional gel electrophoresis. A meta-analysis of DJ-1 two-dimensional electrophoresis profiles found the DJ-1 pool of neuronal tissue to display a characteristic an acidic pI shift associated to

neurodegeneration (Natale et al., 2010). A similar acid shift is observed after cysteine oxidation induced by oxidative stress (Bandopadhyay et al., 2004). DJ-1 was found to have potential sites of oxidation on three highly conserved cysteine residues; C46, C53 and C106. Based on mutational analyses of these sites, C106 was found to be the most important site of oxidative modification and the major player in the acidic pI shift observed under oxidative stress (Canet-Aviles et al., 2004).

The conserved C106 of DJ-1 is thought to be fundamental for normal function of the protein. It lies within a solvent-accessible cleft at the DJ-1 dimer interface, likely to be the active site (Canet-Aviles et al., 2004). Cysteine 106 in is believed to act as an oxidative stress sensor, modulating the protein's activity through reversible stepwise oxidation (Fig 1.2) (Raninga et al., 2017). As oxidative stress levels increase the DJ-1 C106 sulfhydryl is first oxidised to the low activity sulfenic acid form, and then further to the most active sulfinic acid form as reactive oxygen species (ROS) level increases. Further oxidation causes irreversible transition to the inactive sulfonic acid form. The C106 residue can also be S-nitrosylated, enabling DJ-1 to act in transnitrosylation-based regulation of the phosphatase and tensin homolog (PTEN), a key player in neuronal cell death (Choi et al., 2014).
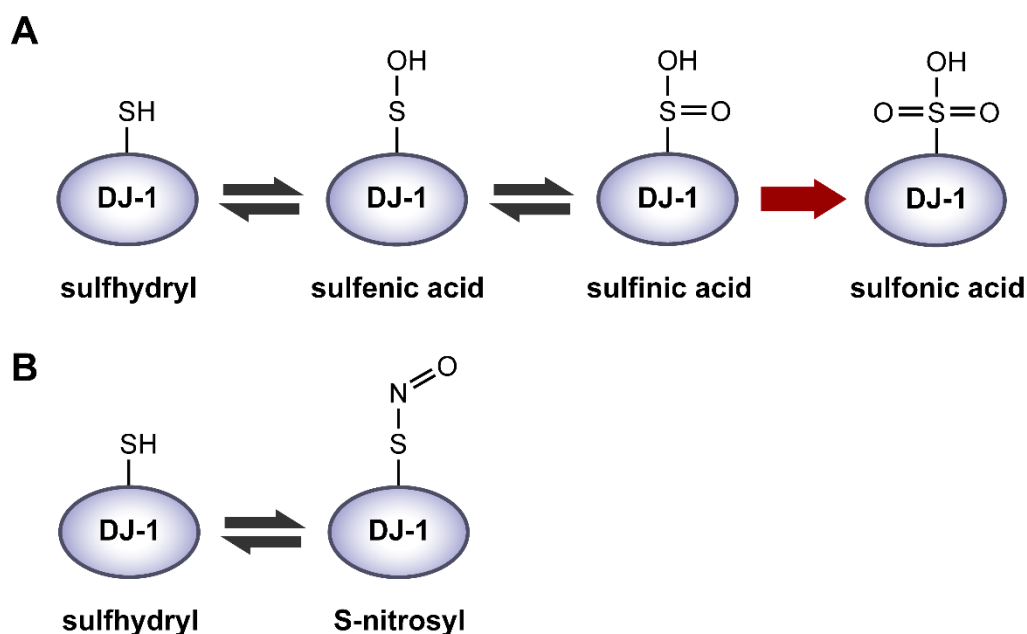
Fig. 1.2 Post-translational modifications of DJ-1 cysteine 106. A: The activity of DJ-1 is modulated through stepwise oxidation of cysteine 106. The transition to the low activity sulfenic acid form and further to the most active sulfinic acid form is reversible, while oxidation to the sulfonic acid form is irreversible and renders DJ-1 inactive. **B:** In addition to oxidation, the Cys106 can undergo S-nitrosylation and transfer the nitrosyl group as part of signalling. From Edson et al. (in press).

1.2.4 DJ-1 in relation to mitochondrial function

As briefly mentioned in section 1.2.2, DJ-1 plays an integral role in regulating mitochondrial homeostasis. DJ-1 has been shown to play an important role in regulation of mitochondrial function and activity with DJ-1 deficiency leading to change in mitochondrial membrane potential, altered morphology, i.e. fragmentation and loss of connectivity, and impaired respiration (Krebiehl et al., 2010, McCoy and Cookson, 2011). Mitochondrial dysfunction has been demonstrated to be age-related and particularly prominent in high energy-demanding tissues in both DJ-1 KO Drosophila and mice (Hao et al., 2010). Oxidation of cysteine 106 to the sulfinic acid form is proposed to be required for DJ-1 to exerts its impact/effect on mitochondria. This has been shown by a DJ-1 mutant unable to form the sulfinic acid form due to alterations to the active site being unable to counter mitochondrial fragmentation despite the presence of C106 (Blackinton et al., 2009). A similar disruption of mitochondrial dynamic is seen with loss of DJ-1, causing increased fragmentation, lowered membrane potential and autophagy (McCoy and Cookson, 2011). Loss of DJ-1 has been shown to affect autophagy in mouse and human cells (Krebiehl et al., 2010). A similar effect was seen in lymphoblasts obtained from familial PD patients belonging to the families where PARK7 was first identified. Here the PD samples had more fragmented mitochondria as well as altered autophagic activity (Irrcher et al., 2010). The DJ-1 mediated regulation of autophagy has been found to involve multiple pathways, notably the ERK and Akt pathways (Oh and Mouradian, 2017).

Endoplasmic reticulum-mitochondria tethering is also affected by DJ-1. Loss of DJ-1 causes reduced contact and reduced Ca^{2+} uptake in the mitochondria. DJ-1 is important for mitochondrial Ca^{2+} homeostasis by facilitating uptake of Ca^{2+} from ER to the mitochondria via specific contact sites (Ottolini et al., 2013).

DJ-1 regulates the activity of complex I of the electron transport chain (ETC) and has been found to bind the complex I subunits ND1 and NDUFS4, promoting stability (Hayashi et al., 2009). DJ-1 deficient cells have also been found to have impaired complex I assembly and supercomplex formation (Heo et al., 2012). Both knockdown and dysfunctional variants of DJ-1 has been reported to result in reduced complex I activity (Hayashi et al., 2009, Zhang et al., 2018). Interestingly, reduced complex I activity has also been linked to the pathogenesis of PD. Both the activity and amount of complex I has been found to be reduced in post-mortem *substantia nigra* of PD patients (Schapira et al., 1990).

1.2.5 Neuroprotective function of astrocytic DJ-1

Astrocytes are highly abundant glia cells and constitute up to 90% of cells in the human brain depending on the region (Park et al., 2012). Not all organisms have the characteristic star-shaped astrocytes found in humans, but nonetheless they still possess cells that serve a corresponding function. The astrocytes play an important role in maintaining redox homeostasis in neurons (Jimenez-Blasco et al., 2015). Reactive oxygen species and nitrogen species (ROS/RNS) are by-products of cellular respiration via the electron transport chain in mitochondria. At moderate levels they play important roles in signalling and regulatory pathways in the cell but at increased levels ROS/RNS may cause damage by oxidising proteins, lipids or DNA (Mailloux et al., 2013). Neurons are especially susceptible to such damage due to their inability to renew themselves, a high basal mitochondrial activity and high lipid content (Salim, 2017).

DJ-1 is found in low levels in neurons, but high levels in astrocytes, and astrocytic DJ-1 appears to play an important role in protecting neurons from oxidative stress (Bandopadhyay et al., 2004). It has been shown that neurons co-cultured with astrocytes have improved survival compared to neuronal monocultures when treated with ROS-inducing stressors (Mullett and Hinkle, 2009). Culturing neurons with astrocyte-conditioned media had a similar protective effect. When neurons were co-cultured with DJ-1 deficient astrocytes however, they were not protected against the ROS-induced cell death, linking the protective effect to astrocytic DJ-1 expression. Frøyset et al. showed that zebrafish with increased astrocytic DJ-1 expression were more resistant to oxidative stressors compared to wild type animals, supporting the redox-regulating role of DJ-1 also *in vivo* (Froyset et al., 2018).

Increased levels of DJ-1 has been found to regulate astrocyte-mediated protection of neurons through different pathways. This includes activation of the antioxidant master regulator Nrf2. By DJ-1 binding to the Nrf2 inhibitor Keap1, Nrf2 is free to translocate from the cytosol into the nucleus (Clements et al., 2006). Here Nrf2 binds antioxidant response elements (ARE), facilitating transcription of the associated genes, which include members of the glutathione pathway such as glutamate cysteine ligase (GCL) and glutathione synthase (GSS), and redox regulating enzymes such as thioredoxin 1 (Trx1), peroxiredoxin 1 (Prx1) and superoxide dismutase 1 (SOD1) (Espinosa-Diez et al., 2015). DJ-1 is also involved in the clearance of excess glutamate from the extracellular space and uptake into the astrocytes via regulation of the channel EAAT2. This prevents glutamate-induced toxicity thus protecting the neurons (Kim et al., 2016). Additionally, the increased uptake of glutamate into the astrocytes aids in the

positive regulation of the Nrf2/Keap1 pathway resulting in upregulation of antioxidant genes and increase in extracellular GSH levels. In this way the antioxidant activity from the astrocytes can match the needs of the neurons as increased neuronal activity leads to increased secretion of glutamate (Habas et al., 2013). Furthermore, DJ-1 has been shown to reduce the activity of induced nitric oxide synthase (iNOS) presumably via inhibition of ASK1 during oxidative stress, thereby preventing excess formation of nitric oxide (NO). At high levels NO may lead to impaired protein function through excessive S-nitrosylation as can be seen in neurodegenerative disorders (Waak et al., 2009). We have summarized the neuroprotective function of astrocyte DJ-1 in Figure 1.3.

The dopaminergic neurons of the *substantia nigra* are particularly sensitive to oxidative stress due to heightened base level mitochondrial oxidative stress (Surmeier et al., 2017) and ROS production being a natural part of dopamine metabolism (Mouradian, 2002). These neurons may therefore be especially dependant on DJ-1 activity despite the levels of DJ-1 in the neurons themselves being relatively low. This sensitivity could explain the selective neurodegeneration seen in PD patients with loss of function DJ-1.
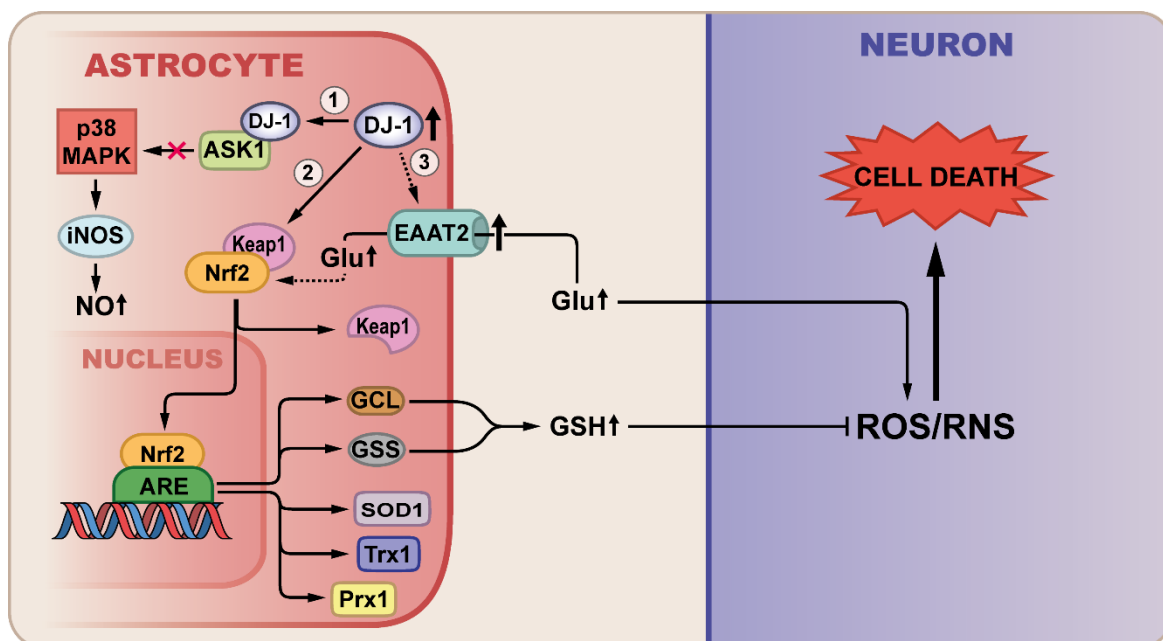
Fig. 1.3 The neuroprotective role of astrocytic DJ-1 under conditions of oxidative stress. Astrocytic DJ-1 acts in a transcellular manner via multiple pathways to reduce oxidative stress in neurons. **(1)** DJ-1 inhibits iNOS-mediated production of NO via inhibition of ASK1. **(2)** Increased transcription of antioxidant genes and oxidative stress response genes via activation of the master regulator Nrf2. **(3)** Increased astrocytic glutamate uptake leading to activation of the Nrf2/ARE pathway and reduced glutamate-mediated cell toxicity. From Edson et al. (in press).

1.3 Neurotoxicant-based models of Parkinson's disease

An important part of research into the underlying mechanisms that lead to PD are the many neurotoxicant-based models of sporadic Parkinson's disease that have emerged over the years. 1-methyl-4-phenylpyridinium ion (MPP^+), 1-methyl-4-phenyl-1,2,3,6-tetrahydropyridine (MPTP), Paraquat, 6-hydroxydopamine (6-OHDA) and rotenone have all been used to model aspects of PD pathogenesis such as the loss of dopaminergic neurons, formation of Lewy bodies and movement dysfunction (Zeng et al., 2018). Although exerted through different modes of action, the common effect of these neurotoxicants is an increase in the intracellular levels of oxidative stress that eventually leads to the PD-characteristic loss of dopaminergic neurons.

Rotenone is a lipophilic compound naturally found in plants of the Derris and Lonchocarpus genus. It has previously been used extensively as a pesticide and piscicide, but the use has since been discontinued in many countries due to its high toxicity, feared environmental impact and ability to induce parkinsonian phenotypes (Heinz et al., 2017).

Rotenone acts on cellular respiration via irreversible inhibition of complex I of the electron transport chain (ETC). By occupying the Co-enzyme Q (CoQ) binding site on Complex I, rotenone effectively prevents binding of CoQ and transport of electrons further down the ETC. This does however not prevent the normal transferring of electrons from NADH into Complex I. With transfer to CoQ blocked, electrons are instead transferred to O_2 in the matrix, forming the initial mitochondrial ROS superoxide ($O_2^{\bullet-}$) (Murphy, 2009). This block in the ETC also leads to reduced production of ATP. Elevated levels of ROS may lead to oxidative damage, lipid peroxidation, defective proteins and DNA damage, and further down the line, mitochondrial dysfunction and apoptosis (Greenamyre and Hastings, 2004).

It is this elevated ROS production that causes the PD-like state. As previously stated, the dopaminergic neurons of the SN are particularly sensitive to oxidative stress (Mouradian, 2002, Surmeier et al., 2017) and increased oxidative stress has been linked to both neurodegeneration and the formation of Lewy bodies (Dias et al., 2013).
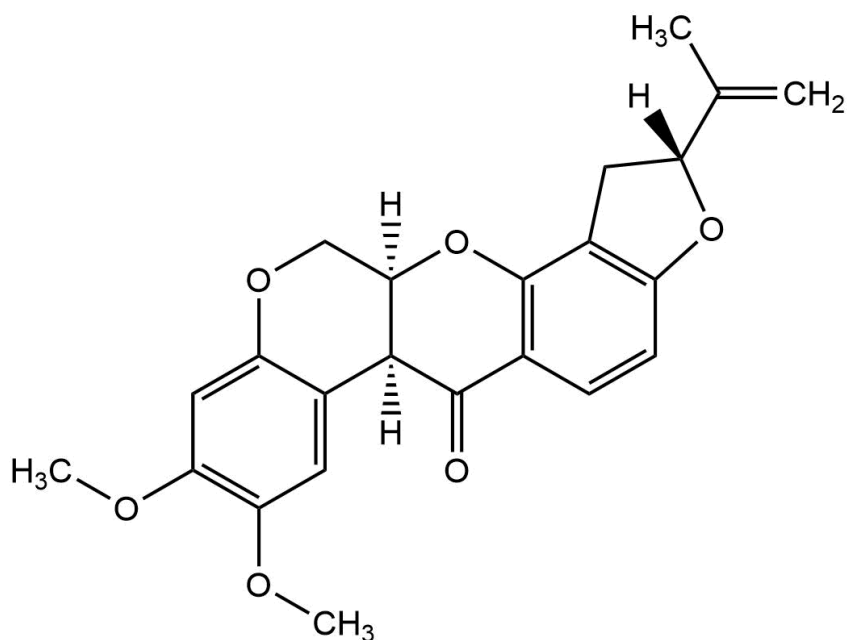
Fig. 1.4 The molecular structure of rotenone

1.4 Zebrafish as a model organism for Parkinson's disease

The zebrafish (*Danio rerio*), a small tropical freshwater fish, is emerging as a popular model organism for human disease. They are convenient animals in that they are easy to house, have a relatively short generation time of approx. 2-3 months and readily reproduce in captivity. Furthermore, a single female may produce up to hundreds of offspring per mating. The external fertilisation makes controlling mating and developmental conditions, as well as experimental treatment of the eggs, far easier than using many other models. Development is rapid with most vital organs formed already 24 hours post fertilization. The eggs themselves and the early embryos are transparent, and embryos/larvae readily take up compounds from the water around them (Santoriello and Zon, 2012). Zebrafish embryos are thus particularly ideal for drug screening, as changes to the developing organs are readily observable in the transparent body (Parng et al., 2002).

In addition to the more practical aspects of using zebrafish as a model organism, there is a high degree of conservation of genome organisation, developmental course as well as signal transduction pathways between zebrafish and humans (Best and Alderton, 2008). It has been estimated that approximately 80% of human disease-related genes have corresponding orthologs in zebrafish (Howe et al., 2013). The overall organisation of the zebrafish brain, as well as many of the defined brain areas are also similar to that seen in humans (Tropepe and

Sive, 2003). Additionally, many of the major neurotransmitter systems, e.g. dopaminergic and noradrenergic, are present (Rink and Wullimann, 2004).

Of particular interest in the context of PD is the ventral diencephalic cluster in zebrafish, seemingly homologous to the midbrain in mammals where the *substantia nigra* is located (Son et al., 2003). The zebrafish homolog of the dopaminergic neuronal marker protein tyrosine hydroxylase (TH), which constitutes the rate limiting step in dopamine synthesis, is also found in the neurons of this area (Holzschuh et al., 2001). As previously stated in section 1.1, it is the loss of dopaminergic neurons in the *substantia nigra* that is the hallmark of PD. Parkinsonian effects such as impaired movement, oxidative stress, mitochondrial dysfunction, selective dopaminergic neurodegeneration and loss of TH has been demonstrated using neurotoxin-induced zebrafish models and genetic/knockdown models (Xi et al., 2011).

1.5 Zebrafish transgenesis via the I-SceI meganuclease system

Mutational analysis using genetically modified animal models overexpressing disease-related genes, expressing mutated variants of these genes or with complete knockouts, have given further insight into their function (Grunwald and Eisen, 2002). The external fertilization, high number of eggs per mating as well as the translucent eggs and embryos make zebrafish ideal animal models for studies based on transgenesis, as microinjections can be performed directly on the egg at the one-cell stage and effects can be observed from this point.

Classical transgenesis, i.e. injecting zebrafish with a transgene-harbouring plasmid only, generally yields a low expression rate. The transgene may initially be expressed at the early stages of development, but not incorporated in the genome so that expression is eventually lost. In the case that the transgene is incorporated, this is often in a mosaic pattern with low germline transmission, so that positive F0 fish only yield a few percent positive offspring. Transgenesis in fish has been greatly improved using the I-SceI enzyme. By co-injecting plasmids harbouring a transgene flanked by the I-SceI recognition site with the I-SceI enzyme at the 1-cell stage both the number of positive F0 fish and the germline transmission is vastly improved, with up to 50% of the F1 generation inheriting the transgene, as well as reduced mosaicism (Thermes et al., 2002).

I-SceI is a meganuclease originally isolated from the yeast *Saccharomyces cerevisiae* with an 18 bp recognition site. Due to the large recognition site, this sequence is expected to occur randomly only once in 7×10^{10} bp and does not occur in the zebrafish genome (Thermes et al., 2002). The mode of action for inserting the cut transgene sequence into the genome is not fully

understood, put is thought to involve I-SceI causing a double-stranded break in the genome. I-SceI was initially used to study homologues recombination, but it's ability to induce a double strand break is likely nonspecific as insertion has been observed at independent sites. By continuously cutting the plasmids at the recognition site, I-SceI counteracts the endogenous ligase activity of the cell, leaving the insert to be integrated via the endogenous repair machinery (Grabher et al., 2004). While other methods such as Tol2 are more prone to multiple insertion events, I-SceI favours single insertions (Grabher et al., 2004).

1.6 The APEX2 system for ultrastructural protein localization

A newly developed tool for ultrastructural protein localization and proteomics is the peroxidase APEX2. It is a 27 kDa modified form of soybean APX with the introduced mutations K14D, W41F, E112K and A134P. These modifications have shown to improve the catalytic properties of APX, further improving its use in electron microscopy and proteomics (Lam et al., 2015). APEX2 catalyses the polymerisation of 3,3'-diaminobenzidine (DAB) in the presence of hydrogen peroxide, forming an insoluble precipitate. This activity is retained in fixed cells and useful for staining as the polymer cannot diffuse and remains at the original site of formation. The polymer is visible by bright-field microscopy. Furthermore, it can be rendered EM-visible by osmium tetroxide treatment as this compound reacts with the DAB polymer, leaving electron-dense osmium (Martell et al., 2017). By engineering fusion constructs of APEX2 and a protein of interest, connected by a flexible linker, the DAB polymer will be distributed in the cell based on the distribution of this protein. This method has previously been demonstrated with the electron microscopy-based determination of the sub-mitochondrial localization pattern of MICU1, a regulatory protein involved in calcium uptake (Lam et al., 2015). APEX2 can also be used to catalyse the biotinylation of proximal endogenous proteins in live cells. This in combination with streptavidin-based chromatography followed by mass spectrometry makes APEX2 fusion proteins useful tools for proximity-based protein mapping (Hung et al., 2016).

1.7 Background and aims of the study

To further our understanding of PD ethology and pathogenesis and the role of DJ-1, two genetically modified zebrafish lines have already been established and characterised in our lab. The first line, UiB1001 (*Tg(gfap:egfp-2A-flag-zDJ-1)*), is a Tübingen AB (TAB) line with astroglial-specific overexpression of DJ-1 driven by elements of the glial fibrillary acidic protein (GFAP) promotor (Froyset et al., 2018). Larvae of this line were found to be protected against MPP$^+$-induced damage related to oxidative stress, demonstrating the protective role of DJ-1 upregulation in astrocytes. Additionally, cell sorting (FACS) followed by protein profiling

of astrocytes overexpressing DJ-1 showed an upregulation of proteins involved in redox regulation, mitochondrial respiration and inflammation.

The second line, UiB2000 ($park7^{-/-}$), is a TAB-based line with complete knockout of DJ-1 (Edson et al., 2019). This line did not display any phenotype at the larval or young adult stage. Older fish however, showed a lowered expression of tyrosine hydroxylase, downregulated mitochondrial complex I activity and a visual phenotype of low body weight and decreased pigmentation, especially in males. Through label-free mass spectrometry of adult brain samples the impact on protein expression was examined. Five main groups of proteins with changed expression compared to wild types were found in the DJ-1 KO fish; protein involved in stress response and vesicle trafficking, the mitochondrial transport chain, glutathione metabolism, inflammation and translational regulation.

Using the already established DJ-1 KO zebrafish line (UiB2000), a line with astroglial-restricted expression of DJ-1 has been established to see if this had a similar protective effect as seen in the astroglial overexpression line UiB1001. Following this we wanted to create a corresponding astroglial-specific DJ-1$_{C106A}$ line to investigate whether the effects of astroglia-restricted expression of DJ-1 were dependent on the C106 residue, i.e. if this line would resemble the KO line or if any of the protective effects of the UiB1001 line would be exhibited.

In addition to developing and characterising the astroglial-specific DJ-1$_{C106A}$ zebrafish line, we wanted to determine the ultrastructural localization of WT DJ-1 and the C106A mutant *in vitro*, and to look for changes in the localization pattern of these two variants in response to rotenone-induced oxidative stress. This would be done first by creating APEX2-linked DJ-1$_{WT/C106A}$ fusion constructs and then using SH-SY5Y cells as an *in vitro* model of neuronal cells in which the fusion constructs could be expressed. The localization pattern of the fusion proteins would then be determined by transmission electron microscopy. The potentially redox-sensitive mitochondrial localization was of particular interest as the results from different studies highly are conflicting. Previous results are mainly based on subcellular fractionation and fluorescence microscopy, thus using APEX2 as a novel approach.

In summary, the principle goal of this thesis was to understand the function of the C106 residue of DJ-1 in oxidative stress response. Our objectives were therefore to:

- Create an astroglial-restricted DJ-1$_{C106A}$ expressing zebrafish line from the established DJ-1KO line.

- Characterise the new line and compare it to the WT, DJ-1 KO and UiB2001 lines in terms of both basal and stress-induced damage and alterations in protein expression.

- Generate a hDJ-1$_{WT}$-APEX2 and hDJ-1$_{C106A}$-APEX2 plasmid constructs.

- Use APEX2 constructs to visualise the ultrastructural localisation pattern of DJ-1$_{WT}$ compared to DJ-1$_{C106A}$ under basal and oxidatively stressed conditions.

2 Materials

2.1 Plasmid constructs

Plasmid	Supplier (Cat. No.)
DsRed2-Mito-7	Addgene (55838)
pcDNA3 APEX2-NES	Addgene (49386)
pcDNA3 Flag-DJ-1$_{WT}$-APEX2-NES	-
pcDNA3 Flag-DJ-1$_{C106A}$-APEX2-NES	-
pBS-ISceI-gfap:eGFP-2A-Flag-zDJ-1$_{WT}$	-
pBS-ISceI-gfap:eGFP-2A-Flag-zDJ-1$_{C106A}$	-

2.2 Primers

Name	Sequence 5' to 3'	Use
E11-DJ106 Fw	TGSTCGCTGCAATCGCTGCAGGCCCG ACGG	Site-directed mutagenesis
E12-DJ106 Rev	CCGTCGGGCCTGCAGCGATTGCAGCG ATCA	Site-directed mutagenesis
E16-DJ Seq 2	CATGGTCCTGCTGGAGTTC	DNA sequencing/ PCR screening
H01_zDJ1_C106A_rev	GACGGCCAGTGAAATTACC	PCR screening
H02_hDJ1_Bsp120I_F	GCGCGGGCCCACCATGGCTTCCAAAA GAGCTCTGG	Restriction-based cloning
H03_hDJ1_Bsp120I_R	GCCGGGGCCCCGCTGCCGCCGCCGCC GTCTTTAAGA ACAAGTGGAGCC	Restriction-based cloning
H04_hDJ1-APEX2_F	GTAACAACTCCGCCCCATTG	DNA sequencing
H05_hDJ1-APEX2_R	GGTGCTTGATGGTTCCGAAG	DNA sequencing

2.3 Enzymes

Name	Type	Restriction site (5'-3')	Supplier (Cat. No.)
Bsp120I	Restriction	G|GGCCC	Thermo Fisher Scientific (ER0131)

I-sceI	Homing meganuclease	TAGGGATAA|CAGGGTAAT	New England Biolabs (R0694S)
KpnI	Restriction	GGTAC|C	New England Biolabs (R0142S)
NcoI	Restriction	C|CATGG	New England Biolabs (R0193S)
NotI-HF	Restriction		
NdeI	Restriction	CA|TATG	New England Biolabs (R0111S)
Shrimp Alkaline Phosphatase (rSAP)	Alkaline phosphatase	N/A	New England Biolabs (M0371S)
T4 DNA Ligase	DNA Ligase	N/A	New England Biolabs (M0202S)
PfuUltra II Fusion HotStart DNA Polymerase	DNA Polymerase	N/A	Agilent Technologies (600670)

2.4 Readymade buffers and media

Name	Supplier (Cat. No.)
CutSmart® Buffer	New England Biolabs (B7204S)
10x DNA Loading Buffer	Takara (9157)
NativePAGE Running Buffer (20X)	ThermoFisher scientific (BN2001)
NativePAGE Sample Buffer (4X)	ThermoFisher scientific (BN2003)
NEBuffer™ I-SceI (10x)	New England Biolabs (B0694)
NEBuffer™ 1 (10x)	New England Biolabs (B7001S)
dNTP mix PCR grade	Roche (11 814 362 001)
Dulbecco's Modified Eagle's Medium - high glucose (DMEM)	Sigma-Aldrich (D6429)
NuPAGE® MES SDS Running Buffer (20X)	Thermo Fisher Scientific (NP0002)

NuPAGE® Transfer Buffer (20X)	Thermo Fisher Scientific (NP0006-1)
10x PfuUltra II reaction buffer	Agilent Technologies (600670)
S.O.C. Medium	Thermo Fischer Scientific (15544034)
T4 DNA Ligase Reaction Buffer	New England Biolabs (B0202S)

2.5 Commercial gels and membranes

Name	Supplier (Cat. No.)
Amersham™ Hybond™ P 0.45 PVDF Blotting Membrane	GE Healthcare Life science (10600023)
NativePAGE™ 3-12% Bis-Tris Protein Gel	Thermo Fisher Scientific (BN1001BOX)
NuPAGE® 4-12% Bis-Tris Protein Gel	Thermo Fisher Scientific (NP0321BOX)

2.6 Molecular size markers

Name	Use	Supplier (Cat. No.)
NativeMark Unstained Protein Standard	Native PAGE protein standard	Thermo Fisher Scientific (LC0725)
PageRuler Plus Prestained Protein Ladder	Western blot protein size marker	Thermo Fisher Scientific (26619)
Quick-Load® Purple 2-Log DNA Ladder	Agarose gel DNA size marker	New England Biolabs (N0550S)

2.7 Bacterial strains

Name	Use	Supplier (Cat. No.)
Escherichia coli Subcloning Efficiency™ DH5α™ Competent cells	Plasmid vector propagation	Invitrogen (18265017)

2.8 Cell lines

Cell line	Derived from	Supplier
SH-SY5Y	Human bone marrow neuroblastoma	ATCC

2.9 Antibodies

Antibody	Dilution	Description	Supplier (Cat. No.)
Primary		Clonality, Host	
Anti-DJ-1	1:3000	Polyclonal, Rabbit	Novous Biological (NB300-270)
Anti-TH	1:10 000	Monoclonal, Mouse	ImmunoStar (22941)
Anti-iNOS	1:2000	Monoclonal, Mouse	BD Biosciences (610431)
Secondary		Clonality, Host, Conjugate	
Anti-Rabbit	1:10 000	Polyclonal, Donkey, HRP	Jackson ImmunoResearch (711-035-152)
Anti-Mouse	1:10 000	Monoclonal, Donkey, HRP	Jackson ImmunoResearch (715-035-150)

2.10 Zebrafish strains and lines

Name	Background strain/line	Genetic modification
UiB1001	TAB	*Tg(gfap:egfp-2A-flag-zDJ-1)*
UiB2000	TAB	*park7$^{-/-}$*
UiB2001	UiB2000	*park7$^{-/-}$,Tg(gfap:egfp-2A-flag-zDJ-1)*
UiB2003	UiB2000	*park7$^{-/-}$,Tg(gfap:egfp-2A-flag-zDJ-1$_{C106A}$)*
Spotty wild type (SWT)	-	-
Tübingen AB (TAB)	-	-

2.11 Commercial kits

Name	Use	Supplier (Cat. No.)
BigDye Terminator v3.1 Cycle Sequencing Kit	DNA sequencing	Applied Biosystems (4337455)

QuickChangeII Site-Directed Mutagenesis Kit	Site-directed mutagenesis	Agilent Technologies (200523-5)
QIAquick® Gel Extraction Kit	DNA extraction from agarose gel	Qiagen (28706)
QIAquick® PCR Purification Kit	DNA purification from PCR	Qiagen (28106)
QIAquick® Spin Miniprep Kit	Bacterial culture miniprep	Qiagen (27106)

2.12 Chemicals and reagents

Chemical	Supplier (Cat. No.)
Acetic acid 100%	Merck KGaA (100063)
Agar 100 Resin	Agar scientific Limited (R1031)
Ampicillin sodium salt	Sigma-Aldrich (A0166-5G)
β-Nicotinamide adenine dinucleotide, reduced disodium salt hydrate	Sigma-Aldrich (N8129-100MG)
Bovine Serum Albumin (BSA)	Sigma-Aldrich (A7906)
Bromophenol blue	Sigma-Aldrich (B0126-25G)
Calcium chloride dihydrate	Merck KGaA (1.02382.1000)
CHAPS	Sigma-Aldrich (C3023)
3,3'-Diaminobenzidine	Sigma-Aldrich (D8001-1G)
Digitonin (5%)	ThermoFisher scientific (BN2006)
Dimethylarsinic acid sodium salt trihydrate	Merck KGaA (8.20670.0100)
Dimethyl sulphoxide (DMSO)	Sigma-Aldrich (D2438)
DL-Dithiothreitol (DTT), min 99% titration	Sigma-Aldrich (D0632)
EDTA	Merck KGaA (108431)
Ethanol	VWR (20821.330)
Ethyl 3-aminobenzoate methanesulfonate salt	Sigma-Aldrich (A5040)
Gelatine capsules	Electron Microscopy Sciences (70103)
Glutaraldehyde 25% solution	Chemi-Teknikk AS (16310)
Glycerine 87%, AnalaR NORMAPUR® analytical reagent	VWR (24385.295)
Glycine	Merck KGaA (104201)

HCl, 37%	Merk KGaA (100317)
Hepes	Merck (110110)
K_2HPO_4	Sigma-Aldrich (P3786)
KH_2PO_4	Merck KGaA (104873)
KCl	Merck (104936)
LB Broth	Sigma-Aldrich (L3022-1KG)
LB Broth with agar (Lennox)	Sigma-Aldrich (L2897-1KG)
Lead (II) nitrate	Merck KGaA (1.07398.0100)
Methanol	VWR (20847.307)
Methylene blue	Merck KGaA (159270.0100)
MgSO4	Sigma-Aldrich (M7506)
NaCl	VWR (27810.295)
NaF, SigmaUltra min. 99%	Sigma-Aldrich (S7920)
Na_3VO_4, min. 90% titration	Sigma-Aldrich (S6508)
Nancy-520	Sigma-Aldrich (01494-500UL)
NativePAGE™ 5% G-250 Sample Additive	Thermo Fisher Scientific (BN2004)
Nitro Blue Tetrazolium chloride, 98+%	Alfa Aesar (J60230)
Osmium tetraoxide	Electron Microscopy Sciences (19134)
Paraformaldehyde	Sigma-Aldrich (P6148)
Phenol red	Sigma-Aldrich (P5530)
PonceauS	Sigma-Aldrich (P3504)
Protease inhibitor cocktail (tablets) complete mini	Roche (118361530012)
Rotenone	MP Biomedicals (150154)
Sodium n-dodecyl sulfate (SDS), 20% aq. soln.	Alfa Aesar (J63394)
Sucrose	Sigma-Aldrich (84100)
SuperSignal™ West Pico PLUS Chemiluminescent Substrate	Thermo Fischer Scientific (34577)
Tri-natriumcitrat di-hydrate	Merck KGaA (567446-1)
Trizma base (H2NC(CH2OH)3)	Sigma-Aldrich (T1503)
Trypsin/EDTA (0.05%/0.02% w/v)	Biochrome (L2153)
TWEEN® 20	Sigma-Aldrich (P5927-500ML)

2.13 Instruments

Name	Use	Manufacturer
Beckman GS-15R Centrifuge	Centrifugation	Beckman Coulter
BIOFUGE pico	Centrifugation	Heraeus
ChemiDoc™ XRS+ Imaging System	Western blot visualisation	Bio-Rad
DNAEngine PTC-200 rev	Polymerase chain reaction, Restriction digestion	Bio-Rad
Electrophoresis power supply - EPS 301	Power supply	Amersham Biosciences
GelDoc™ EZ imager	DNA gel visualisation	Bio-Rad
LEICA M420 Macroscope	Zebrafish larvae imaging	Leica
Multitron Standard incubation shaker	Bacterial shaking incubation	Infors HT
Nanodrop ND-1000™	DNA and protein concentration measurements	Thermo Fisher Scientific
Owl™ EasyCast™ B1 Mini Gel Electrophoresis System	Agarose gel electrophoresis	Thermo Fisher Scientific
Owl™ EasyCast™ B2 Mini Gel Electrophoresis System	Agarose gel electrophoresis	Thermo Fisher Scientific
Picospritzer III-Intracellular microinjection dispense system	Zebrafish egg injection	Parker
SteREO Lumar. V12 Fluorescent microscope	eGFP screening	Zeiss
Reichert Ultracut S Ultramicrotome	Ultrathin sectioning	Leica
VibraCell VCX130, 130 W ultrasonic processor	Homogenization of zebrafish larvae	Sonics
XCell II™ Blot Module	Western Blotting	Thermo Fisher Scientific

XCell SureLock™ Electrophoresis Cell	SDS-PAGE, Native PAGE	Thermo Fisher Scientific
Hoefer SE 260 system	SDS-PAGE	Hoefer Inc
Eppendorf 5810 centrifuge		Eppendorf

2.14 Software and online tools

Name	Use	Developer
EMBOSS Needle	DNA pairwise sequence alignment	EMBL-EBI
Fiji	Protein quantification	LOCI
CLC Main Workbench	DNA sequencing data viewer	Qiagen Bioinformatics
Codon Usage in Homo sapiens	Codon optimization	Codon Usage Database

2.15 Buffers, media and solutions

All buffers, media and solutions are prepared with Milli-Q ultrapure water unless otherwise specified.

2.15.1 Cultivating bacteria

1x LB-Agar

35g/L LB Broth with agar

(Autoclaved)

1x LB medium

35g/L LB Broth

(Autoclaved)

Ampicillin stock (100µg/mL)

100 µg/mL Ampicillin sodium salt

2.15.2 Mammalian cell culturing and experimental treatment

DMEM complete

10% (v/v) Fetal Bovine Serum

1% (v/v) Penicillin-Streptomycin

in DMEM

10x PBS (pH 7.4)

1.55 M NaCl

58 mM $Na_2HPO_4 \cdot 2H_2O$

18 mM KH_2PO_4

27 mM KCl

1x Trypsin solution

0.01% (w/v) Trypsin

0.004% (w/v) EDTA

in 1x PBS (pH 7.4)

Na-Cacodylate buffer (pH 7.4)

0.2 M Dimethylarsinic acid sodium salt trihydrate

0.2 M Sucrose

0.005 M Calciumchlorid-dihydrat

2x Cacodylate buffer (pH 7.4)

4 mM CaCl2 · 2H2O

in 0.2 M Na-Cacodylate buffer

2 % Glutaraldehyde fixation solution

2% (vol/vol) Glutaraldehyde

in 1x Cacodylate buffer

Glycine quenching solution

20 mM Glycine

in 1x Cacodylate buffer

10x DAB solution

5 mg/mL Diaminobenzidine

in 0.1 M HCl

1x DAB staining solution

1x DAB solution

10 μM H_2O_2

1x Cacodylate buffer

2.15.3 Agarose gel electrophoresis

50x TAE

242 g/L Trizma base

50 mM EDTA

57.1 mL/L Glacial acetic acid

2.15.4 SDS-PAGE and western blotting

5x SDS sample buffer

250 mM Tris (pH 6.8)

10 % (w/v) SDS

50 % (v/v) Glycerol

0.025 % (w/v) Bromophenol blue

0.5 M DTT

10x TG

250 mM Trizma base

1.92 M Glycine

1x TGS (Running buffer)

1x TG

0.1% (v/v) SDS

1x TG + methanol (Transfer buffer)

1x TG

10% (v/v) Methanol

Ponceau S solution

0.1% (w/v) Ponceau S

1% (v/v) Acetic acid

in dH$_2$O

1x PBS-T

1x PBS

0.5% Tween

2.15.5 Zebrafish embryo and larvae growth, maintenance and experimental treatment

1x E3 Blank

5 mM NaCl

0.17mM KCl

0.33mM CaCl$_2$

0.33mM MgSO$_4$

1x E3 Blue

5 mM NaCl

0.17mM KCl

0.33mM CaCl$_2$

0.33mM MgSO$_4$

0.01 % (v/v) Methylene blue

10x Injection buffer

0.1 M KCl

0.5% (w/v) phenol red

Injection gel

1.5 % (w/v) agarose

in 1x E3 Blank

Tricaine stock solution (pH 7.0)

4 mg/ml Ethyl 3-aminobenzoate

methanesulfonate salt

21 mM Tris (pH 9)

Tricaine (for euthanasia)

6 ml Tricaine stock solution

in 100 ml fish water

10x PE (pH 7.6)

100 mM K$_2$HPO$_4$

100 mM KH$_2$PO$_4$

10 mM EDTA

Homogenization buffer

1x PE buffer

6 mg/mL CHAPS

50 mM NaF

200 μM NaVO$_4$

1 tablet/25 mL Protease Inhibitor Cocktail

2.15.5 Complex I in-gel activity assay

Complex I homogenization buffer	Complex I substrate solution
3mM EDTA	2mM Tris-HCl (pH 7.4)
250 mM Sucrose	0.1 mg/ml NADH
100mM Hepes (pH 7.5)	2.5 mg Nitro Blue Tetrazolium chloride

3 Methods

3.1.1 T4 DNA ligation

Reactions were prepared with 1x T4 DNA Ligase Reaction Buffer, 100 ng vector, the amount of insert that would yield a 1:3 molar ratio of vector to insert and 1 µL of T4 DNA Ligase to a final of volume of 20 µL. If a higher insert to vector ratio was used this is specified. The reactions were incubated at 16°C O/N.

3.1.2 Heat shock transformation of DH5α bacteria, colony growth and plasmid isolation

50 µl of DH5α cells were thawed on ice for 10 min before gently adding 1-3 µl of ligation reaction or plasmid. Cells were incubated on ice for 30 min, heat shocked for 40 secs in a 42 °C water bath and then immediately put on ice for 2 min. 200 µl of S.O.C. medium was added to the cells before incubating at 37 °C and 250 rpm for 1 hour. 50 and 100 µl of each bacterial preculture were plated on separate LB-Agar plates containing 100 µl/ml ampicillin and incubated at 37 °C O/N.

Colonies were picked from the plates and used to inoculate 4 ml of medium (LB, 100 µg/µl ampicillin) in 15 ml tubes. Tubes were incubated at 37 °C and 250 rpm O/N. A bacteria-free control was prepared and incubated accordingly.

The bacterial O/N cultures were pelleted by centrifugation at 10 000 rpm for 3 min and the supernatant was removed. Plasmid was extracted using the QIAquick® Spin Miniprep Kit following the supplier's manual. The nucleic acid concentration of the plasmid preps was determined using the Nanodrop ND-1000™, with appropriate sample buffer as blank. All following determination of nucleic acid concentration was done accordingly.

3.1.3 DNA sequencing

DNA sequencing was done using the BigDye Terminator v3.1 Cycle Sequencing Kit (Applied Biosystems). Samples were prepared using 1 µl BigDye, 1 µl BigDye Buffer, 200 ng template DNA, and 3.2 pmol of the appropriate forward or reverse sequencing primer, to a final volume of 10 µl.

The cycle sequencing was then run on a thermal cycler using the following program:

Step	Temp	Time
Initial denaturation	96 °C	1 min
Denaturation	96 °C	10 sec
Annealing	50 °C*	5 sec
Extension	60 °C	4 min
Final extension	-	-
Hold	4 °C	∞

Denaturation, Annealing, Extension: 25 cycles

* The standard annealing temperature 50 °C was used unless a sequencing primer-specific annealing temperature (5 °C below primer Tm) is specified

After the PCR was completed, 10 µl of Milli-Q was added to each sample and the samples delivered to the University of Bergen DNA Sequencing Lab for sequencing.

3.1.4 Agarose gel electrophoresis

To visualise DNA, determine the size of and to isolate specific fragments, DNA-containing samples were prepared and separated on an agarose gel. Gels were prepared by dissolving 1% (w/v) agarose in 1x TAE Buffer by repeated boiling in a microwave oven. When the liquid gel mix cooled to 60 °C, 1 µL Nancy-520 was added per 50 mL gel solution and the gel casted in an Owl™ EasyCast™ B1 or B2 Mini Gel Electrophoresis System. Samples were prepared with 1x DNA Loading Buffer (Takara) and run in the Owl™ EasyCast™ B1 or B2 Mini Gel Electrophoresis System with 1x TAE as running buffer at 90-100V until adequate separation. Samples containing 1x Green GoTaq® Buffer were loaded directly onto the gel without adding additional loading buffer. Visualization and imaging were done using the GelDoc™ EZ imager.

3.1.5 Zebrafish care

Adult Zebrafish, larvae and eggs/embryos were kept at the University in Bergen Zebrafish facility following facility guidelines.

Zebrafish mating for experiments or line maintenance was done by keeping the males and females separated O/N in specialized mesh partition boxes. The fish were combined in the top portion of the box the following morning, allowing eggs to collect below the mesh. Eggs were collected with a net and kept in E3 Blue in 10 cm petri dishes in a 28 °C incubator. Eggs to be screened by fluorescence were kept in E3 Blank to avoid background fluorescence.

Adult zebrafish screened negative or to be used for collecting brain and muscle samples were euthanised. The fish were first anesthetized in 100 mL of tricaine solution. When opercular

movement ceased, the fish was placed in a <4°C ice slush for 20 min and then stored at -20°C. Brain and muscle samples were harvested prior to freezing as needed.

3.2 Establishment of the transgenic zebrafish line (UiB2003)

3.2.1 Site-directed mutagenesis: introducing DJ-1 Cys106 to Ala106 mutation to the pBs-ISceI-gfap:eGFP-2A-Flag-zDJ-1 plasmid vector

Mutagenesis and subsequent DpnI-digestion were performed using the QuickChangeII Site-Directed Mutagenesis Kit. 1x reaction buffer, 50ng pBs-ISceI-gfap:eGFP-2A-Flag-zDJ-1 plasmid (Froyset et al., 2018), 125ng of each of the primers E11-DJ106 Fw and E12-DJ106 Rev (see section 2.2), 1 µl PCR grade dNTP mix and 2.5 U PfuUltraII DNA polymerase was prepared to a final volume of 50 µl. A template-free PCR control was prepared accordingly. The reaction was run on a DNAEngine PTC-200 rev thermal cycler using the following program:

Step	Temp	Time	
Initial denaturation	95 °C	30 sec	
Denaturation	95 °C	30 sec	
Annealing	55 °C	1 min	30 cycles
Extension	68 °C	13 min	
Final extension	-	-	
Hold	4 °C	∞	

Both the zDJ-1 Cys106 to Ala106 mutation PCR sample and the control plasmid PCR sample were then incubated with 10 U DpnI for 1 hr at 37 °C in the thermal cycler.

The DpnI-digested mutated plasmid pBS-ISceI-gfap:eGFP-2A-Flag-zDJ-1$_{C106A}$ PCR was used to transform DH5α cells. Bacterial cultures were grown from the resulting pBS-ISceI-gfap:eGFP-2A-Flag-zDJ-1$_{C106A}$-transformed colonies and plasmid samples subsequently prepped from each culture as described in section 3.1.2.

3.2.2 DNA sequencing: Verifying the DJ-1 Cys106 to Ala106 mutation in the pBs-ISceI-gfap:eGFP-2A-Flag-zDJ-1$_{C106A}$ plasmid vector

In order to verify the newly introduced C106A point mutation in the zDJ-1 gene of the pBs-ISceI-gfap:eGFP-2A-Flag-zDJ-1$_{C106A}$ plasmid vector, the zDJ-1 region of the plasmid was sequenced. This was done for each plasmid miniprep as described in section 3.1.2 using the

forward sequencing primer E16-DJ Seq 2 (see table 2.2) and the primer-specific annealing temperature 57°C.

3.2.3 Double digestion of the pBS-ISceI-GFAP:eGFP-2A-Flag-zDJ-1$_{WT}$ and pBS-ISceI-GFAP:eGFP-2A-Flag-zDJ-1$_{C106A}$ plasmids and reinsertion of zDJ-1$_{C106A}$ into the original vector

The mutated plasmid harbouring zDJ-1$_{C106A}$ verified by sequencing and the original zDJ-1$_{WT}$-harbouring plasmid were double digested. For each plasmid, both a 500 ng and 1000 ng plasmid sample were prepared. Samples were prepared with 1x NEBuffer 1, 1x BSA, 500 ng or 1000 ng of plasmid, 2 U KpnI (NEB) and 2 U NcoI (NEB) to a final volume of 20 µL. Digestion was run at 37°C for 1 h.

In order to isolate the desired plasmid fragments, the samples were run on a 1% agarose gel (see section 3.1.4) at 90V for 55 min. 1.5 µg 2-Log NEB ladder was used as standard. The resulting 10500 bp band of the original plasmid and the 1580 bp band of the zDJ-1$_{C106A}$ plasmid were excised from the gel and purified using the QIAquick Gel Extraction Kit (Qiagen) according to the manufacturers protocol.

The plasmid fragments were ligated using T4 ligation (see section 3.1.1) and the resulting ligation mix used to transform DH5α cells. Heat shock transformation and subsequent colony growth and plasmid miniprep was performed as previously described (see section 3.1.2).

3.2.4 Verifying the insertion of zDJ-1$_{C106A}$ in the pBS-ISceI-GFAP:eGFP-2A-Flag- zDJ-1$_{C106A}$ plasmid by PCR screening

The correct reinsertion of the zDJ-1$_{C106A}$-harbouring fragment in the plasmid was verified by PCR screening using primers whose ca. 1000 bp amplicon span the insert-plasmid reinsertion site. Samples were prepared with 1 µL of the newly prepared pBS-ISceI-GFAP:eGFP-2A-Flag-zDJ-1$_{C106A}$ miniprep or 1 µL of a 1:10 dilution of the same miniprep, 1x Green GoTaq$^®$ Reaction Buffer, 1.25 mM MgCl$_2$, 0.2 mM dNTP, 0.5 µM of each of the primers E-16 DJ-1 Seq and H01_zDJ1-C106A_rev (see table 2.2) and 0.5 U of GoTaq$^®$ DNA Polymerase to a final volume of 20 µL. Corresponding samples with the original pBS-ISceI-GFAP:eGFP-2A-Flag-zDJ-1$_{WT}$ plasmid were prepared accordingly as a positive control.

The reaction was run on a DNAEngine PTC-200 rev thermal cycler using the following program:

Step	Temp	Time	
Initial denaturation	95 °C	5 sec	
Denaturation	95 °C	35 sec	
Annealing	56 °C	40 sec	30 cycles
Extension	72 °C	1.5 min	
Final extension	72 °C	5 min	
Hold	4 °C	∞	

Samples were subsequently run on a 1% agarose gel with 1 µg 2-Log NEB ladder as standard at 90V for 1 hour and subsequently imaged (see section 3.1.4).

3.2.5 Injecting DJ-1 KO zebrafish eggs with the pBS-ISceI-GFAP:eGFP-2A-Flag-zDJ-1$_{C106A}$ plasmid for ISceI-based transgenesis to produce the new mutant line

DJ-1 KO fish (*park7$^{-/-}$*) (REF-manuscript) were set up as described in section 3.1.5 to obtain eggs. An injection mix was prepared from 100 ng of pBS-ISceI-GFAP:eGFP-2A-Flag-zDJ-1$_{C106A}$ plasmid, 1x NEBuffer™ I-SceI, 1 µL I-SceI and 1 µL injection buffer to a final volume of 10 µL and loaded into a glass capillary microinjection needle that was then mounted on a Picospritzer III-Intracellular microinjection dispense system. Fertilized eggs were collected and immobilized in the grooves of an injection gel, and immediately injected directly into the cytoplasm at the 1-cell stage with ca. 1.8 nL of the injection mix. Successfully injected eggs were incubated in E3 Blank at 28 °C until screening.

3.2.6 Screening injected embryos for eGFP expression

Following injection, the larvae were screened for enhanced green fluorescent protein (eGFP) expression at 2dpf using a Lumar Zeizz fluorescence microscope. Larvae displaying clear fluorescence in the head, eyes and along the spine were counted as positive, while larvae displaying no fluorescence, only vague fluorescence in the yolk sac or throughout the body, or single patches of fluorescence were counted as negative. Both mosaic and uniform expression larvae were combined and grown to adulthood to produce the F0 generation.

3.2.7 Screening the adult F0 UiB2003 fish by mating with Spotty WT and continuing the line

At 3-4 months old the adult F0 fish were screened by individually mating each fish with Spotty WT fish and subsequently screening the progeny for fluorescence as described in the previous section. Adult fish producing 10-50% positive embryos were combined as the UiB2003 F0 generation. The UiB2003 F0 fish were then outcrossed with UiB2000 *(park7⁻/⁻)* fish, the progeny was screened for fluorescence and positive larvae grown to adulthood. Adult F1 fish were again screened by Spotty WT-mating as previously described. The resulting heterozygous UiB2003 F1 fish were incrossed to yield F2 offspring which were screened for positives at 1 dpf or 2 dpf and used for rotenone experiments or for continuing the line.

3.3 Characterizing the UiB2003 zebrafish line

3.3.1 Effect of rotenone-induced oxidative stress

At 2 dpf, embryos were manually dechorinated using syringe needles and treated at 48 hpf with either 30 nM rotenone or $1.4 \cdot 10^{-4}$% (v/v) DMSO as control. For a single dose-response experiment, groups were treated with 20 nM, 30 nM, 40 nM rotenone or DMSO control. After 24 hours of exposure, the survival and number of larvae afflicted by pericardial and yolk sac edema were determined. Heart rates were measured using a mechanical counter by counting the heart beats over 15 sec for 8 larvae per treatment group. Larvae were imaged at this point using a LEICA M420 Macroscope or harvested for whole larvae protein lysates.

3.3.2 Preparation of zebrafish whole larvae protein lysates by sonication

Larvae were resuspended in 150 µL homogenization buffer and sonicated on ice at 30% amplitude, pulse at 1 sec on/1 sec off, for an effective sonication time of 4x5 sec using a VibraCell VCX130, 130 W ultrasonic processor with a 2 mm sonication probe. Samples were incubated on ice for 15 min, subsequently centrifuged at 16000x g, 4 °C for 10 min, and the supernatant then collected as the final protein lysate. The protein concentration was determined using the Nanodrop ND-1000™ according to the manufacturer's protocol.

3.3.3 Sodium dodecyl sulphate polyacrylamide gel electrophoresis (SDS-PAGE)

To separate proteins from zebrafish whole larvae lysates, samples were prepared with 40 µg protein, 1x SDS sample buffer and Milli-Q to a final volume of 20 µL. The samples were incubated at 95 °C for 5 min and loaded onto either a premade gel or homemade gel. Premade NuPAGE® 4-12% Bis-Tris gels were used to obtain good separation of high kDa target proteins and the gels run in system? At 150V for 1 hour followed by running at 180V.

If homemade gels were used these were prepared as 1 mm thick 10% polyacrylamide running gels using 375 mM Tris-HCl (pH 8.8), 0.1% SDS, 10% acrylamide, 0.05% (w/v) APS, 0.08% (v/v) TEMED and Milli-Q to a final volume of 6 mL. The gel was immediately casted in the Hoefer SE 260 system and isopropanol layered on top to smooth out the gel border. A 4% stacking gel solution was prepared using 125 mM Tris-HCl (pH 6.8), 0.1% SDS, 4% acrylamide, 0.1% (w/v) APS, 0.16% (v/v) TEMED and Milli-Q to a final volume of 3 mL, and immediately casted onto the solidified running gel after removing the isopropanol. Samples were prepared as described above and run on homemade gels in the Hoefer SE 260 system using 1x Running Buffer and run at 20 mA with runtime depending on the kDa of the proteins to be visualised.

3.3.4 Western blotting

A PVDF blotting membrane was primed briefly in methanol, rinsed in deionised water and then kept submerged in blotting buffer until use. NuPAGE® Transfer Buffer was used for premade gels and homemade blotting buffer for homemade gels. Blotting was run at 14V, 4°C O/N in a XCell II™ Blot Module using the aforementioned buffers.

Following blotting, membranes were incubated with Ponceau S for 5 min, rinsed in deionized water and subsequently imaged using the ChemiDoc™ XRS+ Imaging System. Membranes to be probed with anti-DJ-1 were then incubated in 2x blocking solution, while membranes to be probed with anti-iNOS or anti-TH were incubated in 1x blocking solution. Membranes were subsequently incubated with primary antibody; anti-DJ-1 in 1% blocking solution for 1 hr at RT, anti-iNOS or anti-TH in 0.5% blocking solution at 4 °C O/N. Membranes were then washed 4 x 5 min in PBS-T and incubated with secondary antibody, anti-rabbit for DJ-1 and anti-mouse for iNOS or TH, for 1 hr at RT in 0.5% blocking solution. Membranes were again washed 4 x 5 min in PBS-T. Imaging was done using the ChemiDoc™ XRS+ Imaging System after coating the membranes in freshly mixed SuperSignal™ West Pico PLUS Chemiluminescent Substrate.

3.3.5 Complex I in-gel activity assay

Brain and muscle samples were harvested from male adult TAB and UiB2003 F1 fish (see section 3.1.5). Muscle samples were collected from single fish while three brains were combined for each brain sample. 150 µL complex I homogenization buffer was added to each sample and the samples homogenized by 80x punches with an Eppendorf pellet pestle. Additional 150 µL complex I homogenization buffer were added, and the samples centrifuged at 600x g for 10 min at 4 °C. The supernatant was collected as total lysate and subsequently centrifuged at 7000x g for 10 min at 4 °C. The supernatant was discarded, and the pellet

resuspended in 150 µL homogenization buffer before centrifuged at 7000x g for 10 min at 4 °C. The supernatant was again discarded, and the pellet resuspended in 30 µL homogenization buffer to obtain the mitochondrial fraction lysate. The protein concentration was determined using the Nanodrop ND-1000™.

Lysate samples were prepared using 21 µg protein, 1x NativePAGE Sample Buffer and 0.2% Digitonin and subsequently incubated on ice for 20 min followed by centrifugation at 15 000x g for 15 min at 4 °C. The supernatant was collected, and 0.25% G-250 Sample Additive added for a final sample volume of 25 µL. The samples were run on a NativePAGE™ 3-12% Bis-Tris Protein Gel in an XCell SureLock™ Electrophoresis Cell with 1x NativePAGE Running Buffer on ice for 30 min at 150V followed by 60 min at 250V. NativeMark Unstained Protein Standard was used as standard.

Fresh Complex I substrate solution was prepared, and the gel incubated in this solution for approx. 15 min until bands were visible. The reaction was stopped with 10% acetic acid and the gel imaged using the ChemiDoc™ XRS+ Imaging System.

3.4 Generating fusion constructs for determination of ultrastructural localization of DJ-1 using APEX2.

3.4.1 Generating hDJ-1$_{WT}$ and hDJ-1$_{C106A}$ inserts for APEX2 plasmid

In order to prepare the hDJ-1$_{WT}$ and hDJ-1$_{C106A}$ ORFs for insertion into the pcDNA3 APEX2-NES plasmid the desired modifications to the sequences were generated via PCR. Samples were prepared with 1x PfuUltra II reaction buffer, 0.25 mM dNTPs, 100 ng of the respective template plasmids harbouring hDJ-1$_{WT}$ and hDJ-1$_{C106A}$, 0.4 µM of the forward primer H02_hDJ1_Bsp120I_F and 0.4 µM of the reverse primer H03_ hDJ1_Bsp120I_R (see section 2.2) and 1 µL of PfuUltra II Fusion HotStart DNA Polymerase to a final volume of 25 µL. The reaction was run on a DNAEngine PTC-200 rev thermal cycler using the following program:

Step	Temp	Time	
Initial denaturation	95 °C	2 min	
Denaturation	95 °C	20 sec	
Annealing	60 °C	20 sec	30 cycles
Extension	72 °C	15 sec	
Final extension	72 °C	3 min	
Hold	4 °C	∞	

Samples were subsequently analysed by agarose gel electrophoresis to verify the amplification of the desired fragment. A Nancy-520-stained 1% agarose gel was used with 10 µL Quick-Load® Purple 2-Log DNA Ladder as standard and electrophoresis run at 100V for 1.5 hours (see section 3.1.4). An identical PCR was run, and the resulting samples purified using the QIAquick® PCR Purification Kit (Qiagen) according to the manufacturers protocol.

3.4.2 Introducing hDJ-1$_{WT}$ and hDJ-1$_{C106A}$ to the pcDNA3 APEX2-NES plasmid by restriction digestion and subsequent DNA ligation

Digestion reactions were prepared for each of the hDJ-1$_{WT}$ and hDJ-1$_{C106A}$ purified PCR products using 1 µg PCR product, 10 mM Tris-HCl buffer (pH 7.55 at 37 °C), 10 mM MgCl$_2$, 0.1 mg/mL BSA and 10 U Bsp120I to a final volume of 50 µL. Digestions were incubated at 37 °C for 16 hours and then heat inactivated at 80 °C for 20 min. The digested samples were then run on a 1 % agarose gel at 90V for 50 min (see section 3.1.4) and the digested fragments excised from the gel and purified using the QIAquick Gel Extraction Kit (Qiagen) according to the manufacturers protocol.

A second digestion mix was prepared with 1x CutSmart® Buffer, 1 µg of pcDNA APEX2-NES plasmid and 10 U NotI-HF to a final volume of 50 µL. This reaction was incubated for 15 min at 37 °C and then heat inactivated at 65 °C for 20 min. 2.5 U of rSAP was then added to the sample and incubated at 37 °C for 30 minutes before heat inactivation at 65 °C for 5 min.

The Bsp120I-digested hDJ-1$_{WT}$ and hDJ-1$_{C106A}$ inserts were introduced to the NotI-digested and dephosphorylated pcDNA3 APEX2-NES plasmid using T4 ligation (se section 3.1.1) with an insert to vector molar ratio of 1:6.

The ligation mix was used to transfect DH5α cells and the subsequent colony and culture growth and following miniprep done as previously described (see section 3.1.2).

3.4.3 Screening minipreps for plasmids with correct insertion by restriction analysis

Each of the pcDNA3 DJ-1WT-APEX2-NES and pcDNA3 DJ-1C106A-APEX2-NES plasmid mini preps were analysed by restriction digestion using NdeI. Samples were prepared with 1x CutSmart® Buffer, 500-600 ng of plasmid and 5 units of NdeI to a final volume of 25 µL and subsequently incubated at 37°C for 40 min.

The digested samples were loaded onto a 1% agarose gel and run at 90V for approx. 2.5 hour and imaged as described in section 3.1.4. 15 µL Quick-Load® Purple 2-Log DNA Ladder was used as standard.

3.4.4 Verification of the pcDNA3 DJ-1$_{WT}$-APEX2-NES and pcDNA3 DJ-1$_{C106A}$-APEX2-NES fusion constructs by DNA sequencing

In order to verify the successful introduction of the hDJ-1$_{WT/C106A}$ genes as well as the correct orientation of the genes in the pcDNA3 APEX2-NES plasmid vector, all plasmids screened positive or ambiguous via restriction analysis were sequenced as described in section 3.1.3 using the forward sequencing primer H04_DJ1-APEX2_F and the reverse primer H05_DJ1-APEX2_R (see table 2.2).

3.5 Ultrastructural analysis of DJ-1$_{wt}$ and DJ-1$_{C106A}$ cellular localization

3.5.1 Seeding

One day prior to transfection a 90-100% confluent 10 cm dish of SH-SY5Y cells was removed from the incubator and the medium gently removed by aspiration. The cells were rinsed with 1x PBS and 1x Trypsin solution added dropwise directly onto the cell layer and the cells incubated for approx. 2 min in a 37°C, 5% CO_2 incubator until detaching. The trypsination was stopped by adding fresh DMEM complete at 10 times the volume of the 1x Trypsin solution and the cell suspension was collected. The cells were pelleted by centrifugation at 160 x *g* for 5 min, the medium discarded, and the pellet resuspended in 6 mL DMEM complete. To obtain 70-80 % confluence in each well of a 6-well plate on the following day, 600-700 µL of this cell suspension was added to 1.5 mL DMEM complete per well. The appropriate cell suspension volume for seeding was determined empirically for each cell batch prior to running the experiment.

3.5.2 Transfection

24 h after seeding, the cells were co-transfected with 2 µg of pcDNA3 hDJ-1$_{WT}$-APEX2-NES or pcDNA3 hDJ-1$_{C106A}$-APEX2-NES and 2 µg of DsRed2-Mito-7 using Lipofectamine 1000 following the manufacturers protocol. The DMEM complete was replaced with antibiotic-free, serum-free DMEM prior to adding the transfection complexes and the cells were incubated in this transfection medium for 6 h at 37 °C and 5 % CO_2 before replacing the medium with DMEM complete and continuing the incubation O/N. A non-transfected control was prepared accordingly.

3.5.3 Rotenone treatment

24 h after transfection the transfection medium was replaced with DMEM complete medium containing 250 nM rotenone and 0.0011% (v/v) DMSO or 0.0011% (v/v) DMSO only. Cells were exposed to the respective treatments for 24 h.

3.5.4 Fixation and diaminobenzidine-staining

The cells were removed from the incubator and the cell medium replaced with 800 µL of 37 °C prewarmed 2 % glutaraldehyde solution. The glutaraldehyde solution was immediately replaced with 1.2 mL fresh 2 % glutaraldehyde solution and the cells placed on ice. All following steps were performed on ice. After 60 min of fixation, the glutaraldehyde solution was removed, and the cells were washed 5 x 2 min with 2 mL of 1x cacodylate buffer. The buffer was then replaced with 2 mL of the 20 nM glycine quenching solution and the cells incubated on ice for 5 min and again washed 5 x 2 min with 2 mL of 1x cacodylate buffer. The washing buffer was removed and replaced with 3 mL of 1x DAB solution (10 mM H_2O_2) and the cells incubated for ca. 10 min until the DAB reaction product could be visualized by light microscopy. Cells were washed 5 x 2 min with 2 mL of 1x cacodylate buffer and subsequently imaged using a light microscope.

3.5.5 Transmission electron microscopy

To prepare the DAB stained cells for transmission electron microscopy, cells were post fixed with 1% osmium tetraoxide in 0.1 M sodium cacodylate buffer for 1 hour. Following post fix cells were rinsed twice with 0.1 M sodium cacodylate buffer. The cells were then dehydrated by incubation in increasing concentrations of ethanol; 20 min in 35% ethanol, 20 min in 50% ethanol, 20 min in 70% ethanol, 20 min in 96% ethanol and finally 3 x 20 min in 100% ethanol. All steps up until dehydration with 70% ethanol were done on ice. The cells were then set in a 1:1 mix of Agar 100 Resin and ethanol for 1 hour at 37 °C. The liquid was removed and immediately replaced with a thin layer of 100% Agar 100 Resin and the samples incubated at 37°C O/N. Gelatine capsules were then pressed into the cell layer and the samples incubated at 60°C O/N. The capsules were filled with resin and left to polymerise at 60°C for 2 days. The capsules were broken off the wells of the 6-well cell plate and the cell monolayer cut into 60 nm thin sections using a Reichert Ultracut S Ultramicrotome. The sections were subsequently stained 20 min with 2% uranylacetat and rinsed in Milli-Q. Lead citrate staining solution was prepared as described by Reynolds (Reynolds, 1963) and sections stained for 10 min. Finally, imaging was done using a JEM-1230 Transmission Electron Microscope with an integrated GATAN multi scan camera.

4 Results

4.1.1 Verification of site-directed mutagenesis

In order to create a plasmid vector for generating zebrafish with astroglial over-expression of mutant (C106A) DJ-1, a Cys106 to Ala106 mutation was introduced to the DJ-1 ORF of the pBs-ISceI-gfap:eGFP-2A-Flag-zDJ-1 plasmid by site-directed mutagenesis (Fig. 4.1). The plasmid contains regulatory components of the glial fibrillary acidic protein (GFAP) promotor which gives an astroglial-specific expression pattern (Froyset et al., 2018, Bernardos and Raymond, 2006).
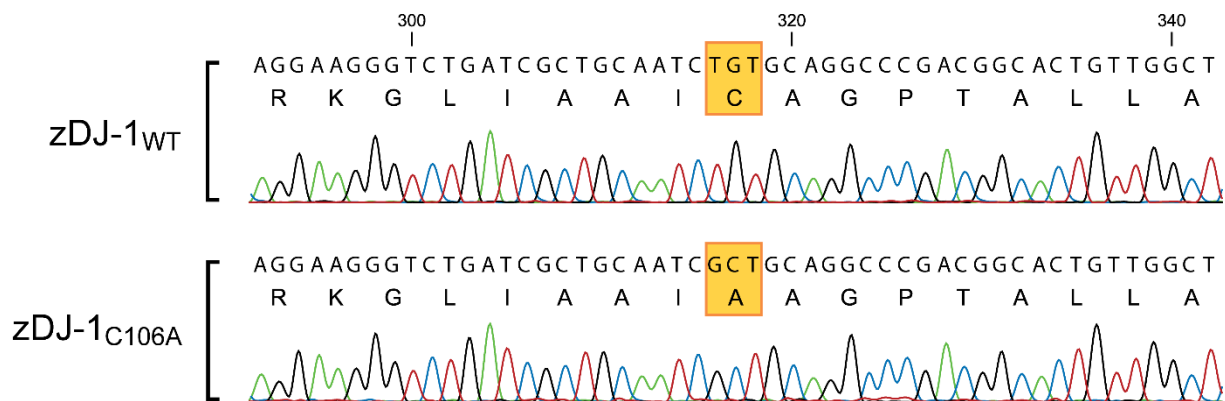

Fig. 4.1 Sequencing alignment of zDJ-1$_{WT}$ and zDJ-1$_{C106A}$. The introduction of a C106A mutation to the DJ-1 ORF of the pBS-ISceI-gfap:eGFP-2A-Flag-zDJ-1$_{WT}$ plasmid by site-directed mutagenesis was verified by DNA sequencing. The site of the mutation is indicated by an orange box with the wild type variant TGT (Cys) shown in the upper sequence and the mutated variant GCT (Ala) shown in the lower sequence.

4.1.2 Generation of zebrafish with astroglial over-expression of DJ-1$_{C106A}$

In order to validate successful incorporation of gfap:eGFP-2A-Flag-zDJ-1$_{C106A}$ into the DJ-1 knock-out line (Edson et al., 2019) larvae were screened for expression of the reporter protein eGFP. Due to the viral 2A segment between eGFP and DJ-1$_{C106A}$, the two proteins are expressed in equimolar amounts as two separate proteins. Thus, fluorescence-validated expression of eGFP is assumed to correspond to the expression pattern of DJ-1$_{C106A}$.

Due to the possibility that F0 fish screened positive at the larval stage are not able to transfer the transgene to their offspring, either as a result of mosaicism or temporary expression of plasmids not incorporated in the genome at the time of screening, the adult F0 fish were screened by Spotty WT mating (Fig. 4.2). The proportion of eGFP-positive embryos produced by each outcrossed fish varied greatly, with the majority of fish producing no positive offspring

or very low levels of positive offspring (1-5%), indicating mosaic expression of the transgene. Only a single male F0 fish produced the 50% positive offspring expected of mendelian single gene inheritance from a heterozygous individual. At the F1 generation, however, all screened *park7^{-/-},Tg(gfap:egfp-2A-flag-zDJ-1_{C106A})* (UiB2003) fish were positive and displaying the expected mendelian inheritance.
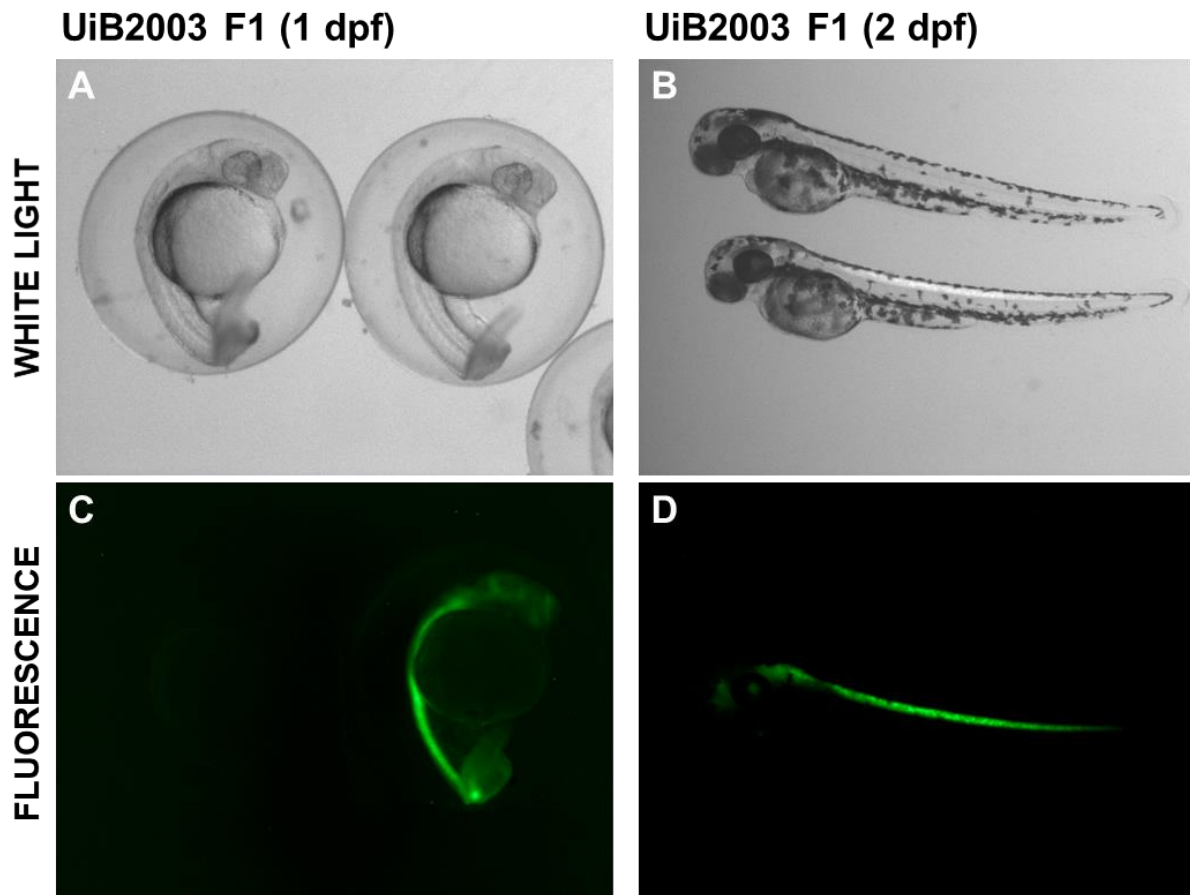

Fig. 4.2 Astroglial eGFP expression in *park7^{-/-},Tg(gfap:egfp-2A-flag-zDJ-1_{C106A})* **(UiB2003) larvae.** UiB2003 F1 embryos at 1 dpf (A and C) and 2 dpf (B and D) comparing eGFP-positive and negative embryos. The same embryos are imaged with A-B: white light and C-D: fluorescence images of 1 dpf (A and C) and 2 dpf (B and D) embryos. Panels shows both eGFP positive and negative embryos. The 2 dpf embryos were dechorinated prior to imaging. As seen in panel C-D, eGFP expression is found in the head region and spinal cord of positive embryo from 1 dpf. At 2 dpf eGFP is also visible in the retina (D).

4.1.3 Verification of Flag-tagged DJ-1$_{C106A}$ expression

Astroglial DJ-1$_{C106A}$ expression in the DJ-1 wild type null background was verified at the protein level by Western blotting (Fig. 4.3). The endogenous DJ-1 protein has an expected size of approx. 20 kDa, while the size of Flag-tagged DJ-1 is approx. 22 kDa. Figure 4.3 shows that UiB2003 expresses Flag-DJ-1 with no endogenous DJ-1 background. The figure also shows endogenous DJ-1 and Flag-DJ-1 expression in lysates from *Tg(gfap:eGFP-2A-Flag-zDJ-1)* (UiB1001) and DJ-1 KO (*park7$^{-/-}$*) (UiB2000) for comparison.

UiB2003 had a higher expression of Flag-tagged zDJ-1$_{C106A}$ compared to the Flag-tagged zDJ-1$_{WT}$ in the UiB1001 larvae. Flag-tagged zDJ-1$_{WT}$ level in isolated astroglial cells from UiB1001 has previously been shown to be approx. 10-times higher than the endogenous DJ-1 level (Frøyset et al., 2018). Thus, it appears that the astroglial zDJ-1$_{C106A}$ level in the UiB2003 larvae far exceeds the endogenous DJ-1 in astroglial cells.
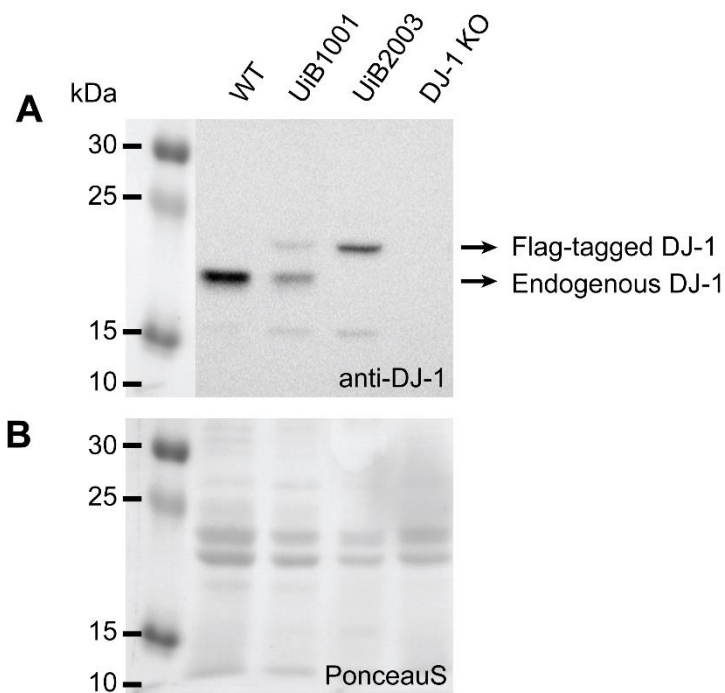

Figure 4.3 DJ-1 expression in transgenic larvae
A: Lysates from 3 dpf larvae were separated by SDS-PAGE and analysed by Western blotting using a DJ-1 antibody which detects both endogenous and Flag-tagged DJ-1. Expression of Flag-tagged DJ-1$_{C106A}$ (approx. 22 kDa), but not endogenous DJ-1 (approx. 20 kDa), was observed in the UiB2003 larvae. The astroglial DJ-1 overexpression line UiB1001 was used as a reference as it possesses both the endogenous DJ-1 and the Flag-tagged DJ-1. **B**: Ponceau S staining of the membrane. Ponceau S was used as a loading control.

4.2 Sensitivity of transgenic lines to oxidative stress

4.2.1 Oxidative stress induced changes in gross anatomy and heart rate

To test if the established transgenic lines had a different tolerance for oxidative stress we exposed larvae to the mitochondrial complex I inhibitor rotenone for 24 hrs starting at 2 dpf. Larvae from WT, DJ-1 KO *(park7$^{-/-}$)* (UiB2000), UiB2001 (*park7$^{-/-}$,Tg(gfap:egfp-2A-flag-zDJ-1)*) and UiB2003 (*park7$^{-/-}$,Tg(gfap:egfp-2A-flag-zDJ-1$_{C106A}$)*) that were exposed to rotenone all exhibited pericardial (P.E.) and yolk sac edema (Y.E.) and pronounced development defects as e.g. bent spines (Fig. 4.4). These phenotypes were not observed in unexposed larvae (Fig. 4.4 A, C, E, and G).

Rotenone also affected survival rates of the embryos (Figure 4.5 A). Interestingly, only larvae with astroglial DJ-1$_{WT}$ or mutant DJ-1 showed a significant decrease in survival rate, whereas DJ-1 knock-out larvae did not. Additionally, both these two lines showed more pronounced rotenone induced edema compared to DJ-1 knock-out larvae (Figure 4.5 B).
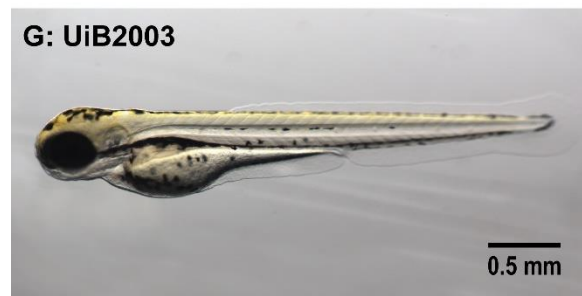
DMSO   **30 nM rotenone**
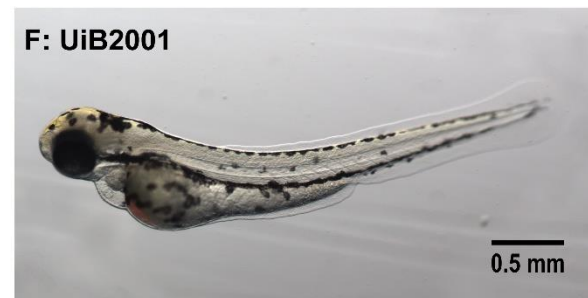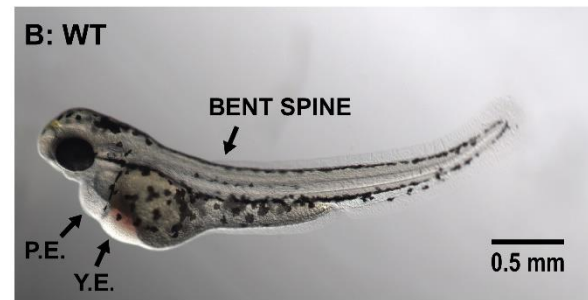
Fig. 4.4 Phenotypic defects of rotenone exposure. Dechorinated WT, DJ-1 KO *(park7⁻/⁻)* (UiB2000), UiB2001 *(park7⁻/⁻,Tg(gfap:egfp-2A-flag-zDJ-1))* and UiB2003 *(park7⁻/⁻,Tg(gfap:egfp-2A-flag-zDJ-1_{C106A}))* larvae were treated with 30 nM rotenone (B, D, F and H) or DMSO control (A, C, E and G) at 2 dpf. Larvae were imaged 24 h after exposure. Defects such as pericardial (P.E.) and yolk sac edema (Y.E.), and a bent spine were found within all rotenone-treated groups. Examples of these defects are indicated in panel B by arrows. DMSO-treated control groups did not display rotenone-induced phenotypes. A scalebar (0.5 mm) is indicated in each panel.

Rotenone decreased the heart rate of the exposed larvae from both wild type and transgenic animals (Figure 4.5 C). This effect was less pronounced in DJ-1 knock-out larvae compared to wild type and larvae selectively expressing DJ-1 or mutant DJ-1 in astroglia (Figure 4.5 C).
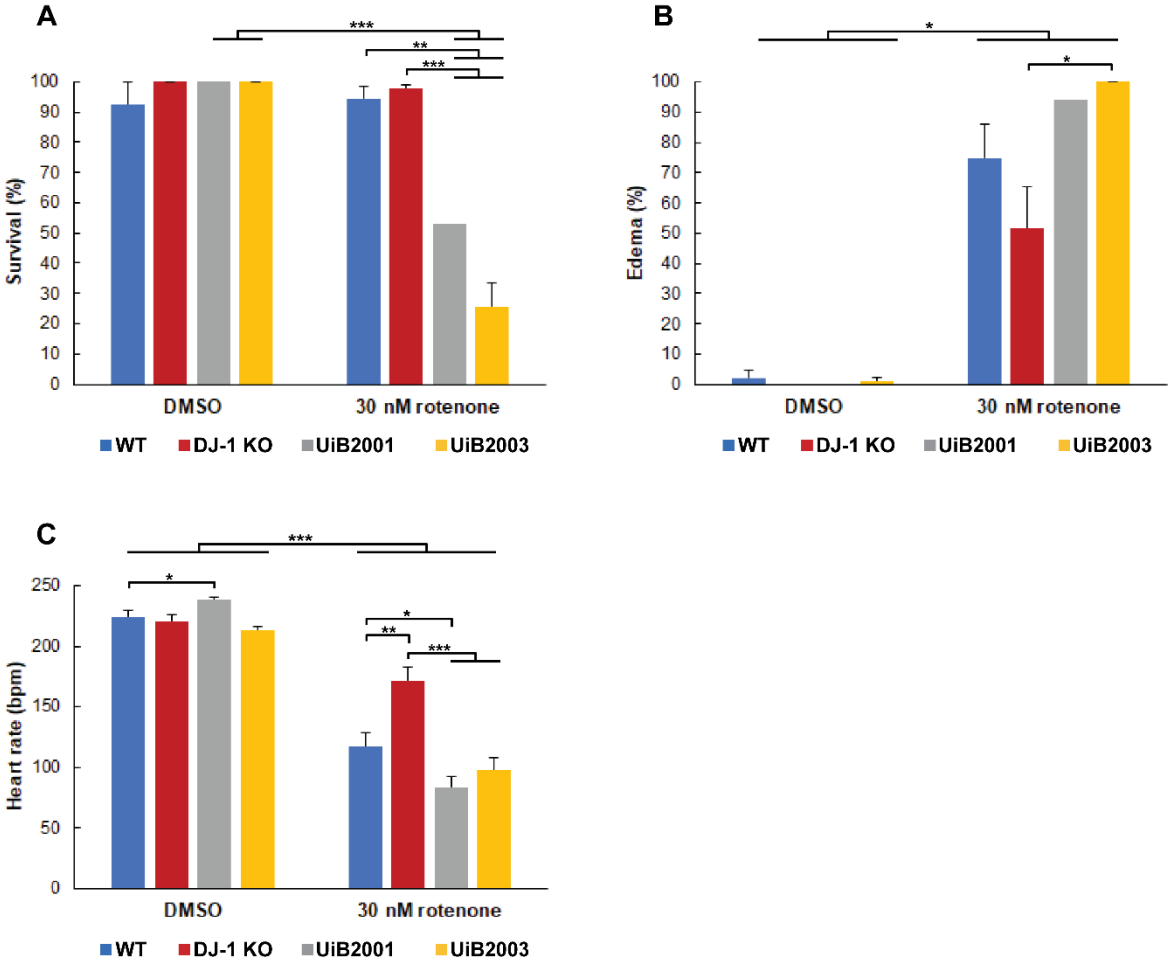
Fig. 4.5 Exposure to rotenone at the embryonic stage is detrimental to larval development and survival, with severity dependant on DJ-1 expression. Dechorinated WT, DJ-1 KO *(park7⁻/⁻)* (UiB2000), UiB2001 *(park7⁻/⁻,Tg(gfap:egfp-2A-flag-zDJ-1))* and UiB2003 *(park7⁻/⁻,Tg(gfap:egfp-2A-flag-zDJ-1$_{C106A}$))* larvae were treated with 30 nM rotenone or DMSO control at 2 dpf. After 24 h of exposure heart rate (bpm) (A), developmental defects in the form of pericardial and yolk sac edema (B), and survival (C) was determined. Data on survival and edema is presented as mean percentage (n=2) for UiB2001 and rotenone-treated UiB2003, and mean percentage (n=3) + SEM for the remaining groups, with data obtained from individual experiments with 15-30 larvae per treatment group. Heart rate data is presented as mean bpm (n=16-24) + SEM from the same experiments. P values were determined by two-tailed t-Test with $p<0.05$ (*), $p<0.01$ (**) and $p<0.001$ (***).

4.2.3 Effect of oxidative stress on protein expression in transgenic lines

Following the determination of heart rate, survival and gross anatomy after rotenone exposure, the surviving larvae were harvested and whole larvae lysates prepared and analysed by Western blotting (Fig. 4.6). The expression of tyrosine hydroxylase (TH), a marker protein of dopaminergic neuronal health, and inducible nitric oxide (iNOS), a marker for intracellular oxidative stress, were examined, quantified and normalised to the overall loaded protein amount using Ponceau S bands. The nitric oxide synthase antibody used detects three different isoforms of NOS; nNOS, eNOS and iNOS. Only the inducible form, iNOS, is addressed in this study (indicated by asterisk). Figure 4.6 panel A and B shows representative blots of rotenone effect on TH and NOS expression respectively while panel C and D show the corresponding quantitation of Western blots probed for these proteins. As seen in Fig. 4.6 panel C, the WT larvae showed a markedly lower TH level in rotenone-treated larvae compared to controls ($p < 0.01$) while the same effect could not be seen for DJ-1 KO, UiB2001 or UiB2003 larvae. DMSO-treated UiB2003 larvae however, showed significantly lower ($p < 0.05$) TH levels compared to DMSO-treated WT larvae. In the case of iNOS expression (panel D), an elevated level was observed in rotenone-treated DJ-1 KO larvae compared to the treated WT larvae ($p < 0.05$). Rotenone-treated UiB2003 larvae on the other hand had a significantly lower iNOS level than the rotenone-treated DJ-1 KO ($p < 0.05$).
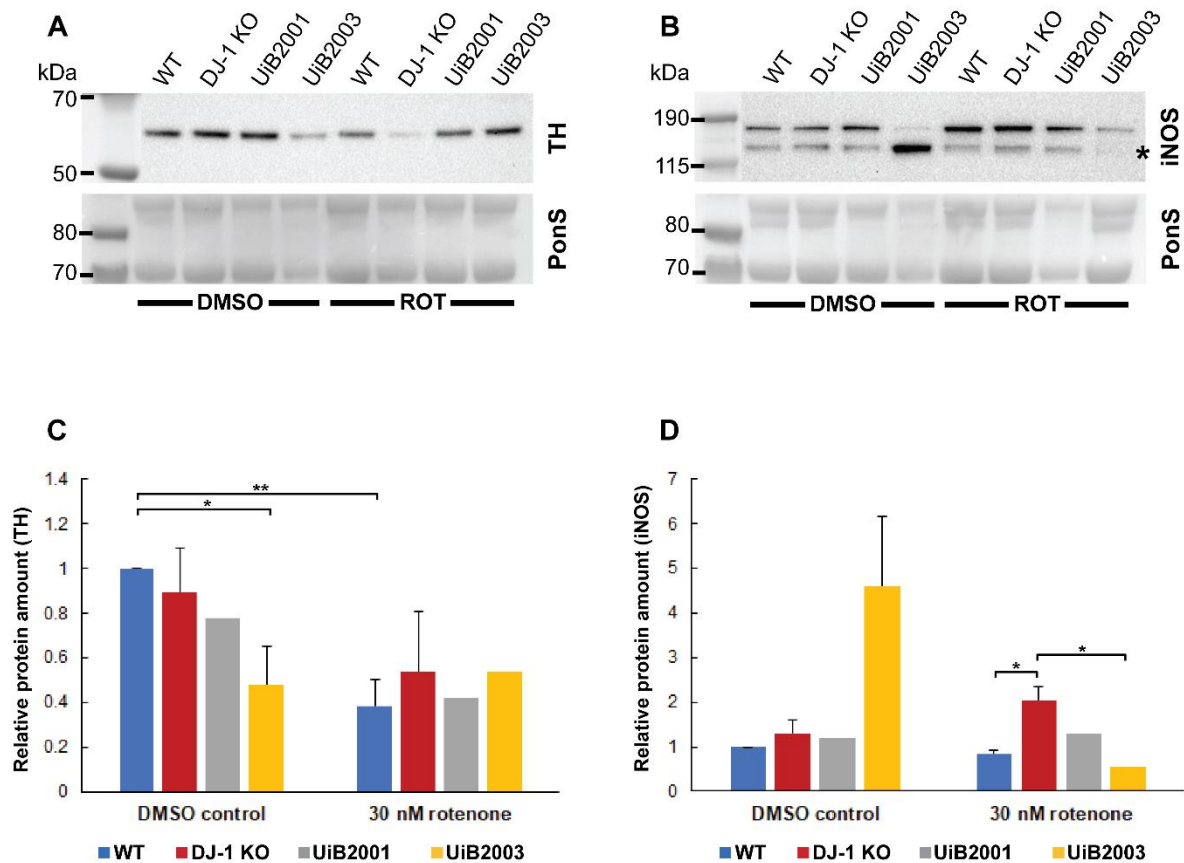
Fig. 4.6 Effect of rotenone exposure on tyrosine hydroxylase and inducible nitric oxide synthase. WT, DJ-1 KO *(park7⁻ᐟ⁻)* (UiB2000), UiB2001 *(park7⁻ᐟ⁻,Tg(gfap:egfp-2A-flag-zDJ-1))* and UiB2003 *(park7⁻ᐟ⁻,Tg(gfap:egfp-2A-flag-zDJ-1_C106A))* larvae were exposed to 30 nM rotenone or vehicle from 2 to 3 dpf. Protein lysates from whole larvae were separated by SDS-PAGE and analysed by Western blotting using antibodies towards tyrosine hydroxylase (TH) and nitric oxide synthetase (NOS). The latter detects nNOS, eNOS, and iNOS (indicated by asterisk). Panel A and B show representative blots of TH and NOS respectively, in which Ponceau-S is used as loading control. Panel C and D show quantitation of Western blots probed with anti-tyrosine hydroxylase (C) and anti-nitric oxide synthase (D) in which Ponceau S staining was used as a loading control. Data are the mean (n=2) for UiB2001 and rotenone-treated UiB2003, and mean (n=3) + SEM for the remaining groups, of three individual experiments with 15-30 larvae per treatment group. P values were determined by two-tailed t-Test with p<0.05 (*) and p<0.01 (**).

4.2.4 Rotenone dose-response of transgenic lines

As 30 nM rotenone resulted in increased larvae deaths a dose-response experiment was performed. Larvae were exposed for to 20 nM, 30 nM or 40 nM rotenone or vehicle for 24 hrs starting at 2 dpf and the survival rate and edema determined (Fig. 4.7). Both WT and DJ-1 KO larvae showed a similar response with no death or edema at the lowest concentration, moderate edema rate but no death at 30 nM rotenone and high edema rate but low death at 40 nM. The UiB2003 larvae seemed to be more sensitive to rotenone. At 20 nM rotenone 100% of larvae were afflicted by edema and at 30 nM the majority of the larvae were dead. At 40 nM none of the UiB2003 larvae survived. All control groups were unaffected with a 100% survival rate.
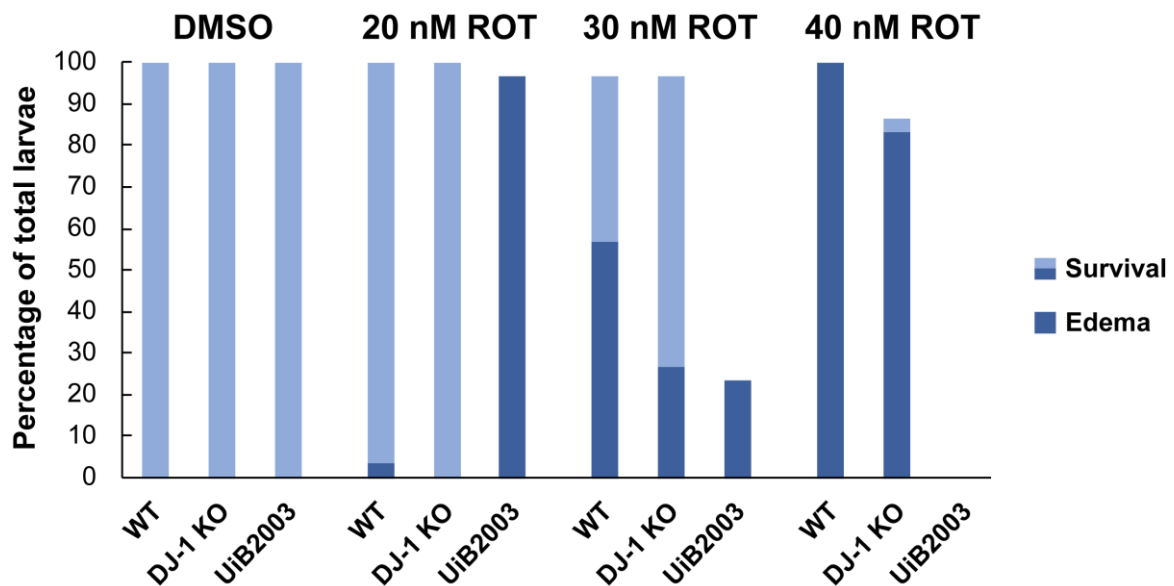
Fig. 4.7 Preliminary dose-response experiment shows UiB2003 larvae to be more sensitive to rotenone than both WT and DJ-1 KO larvae WT, DJ-1 KO *(park7⁻/⁻)* (UiB2000) and UiB2003 (*park7⁻/⁻,Tg(gfap:egfp-2A-flag-zDJ-1_{C106A})*) zebrafish embryos were treated at 2 dpf with 20, 30, or 40 nM of rotenone or with DMSO as negative control. After 24 hrs of treatment the survival rate and number of larvae displaying pericardial and yolk sac edema was determined. Each bar represents the percentage of survival in a group after exposure to the indicated treatment, while the dark portion of each bar represents the percentage of the live larvae afflicted by pericardial and yolk sac edema within this group. The data presented was obtained from a single experiment in which n=30.

4.2.5 Effect of astroglial-restricted DJ-1$_{C106A}$ on Complex I activity

DJ-1 has been shown to regulate the activity of mitochondrial complex I of the electron transport chain. Whether this regulation is dependent of C106 oxidation of DJ-1 is not known. To investigate if the complex I activity of UiB2003 fish was affected by the astroglial-restricted expression of DJ-1$_{C106A}$, total lysates and mitochondrial fraction lysates from adult WT and UiB2003 fish were separated by native page and complex I activity analysed by an in-gel complex I activity assay (Fig. 4.8). Figure 4.8 shows that complex I activity appears in several bands in the native gel. The bands represent both complex I alone and in supercomplexes with mitochondrial complex III, and IV. The lack of endogenous DJ-1 in skeletal muscle of UiB2003 reduced mitochondrial complex I activity as compared to control animals. Mitochondria isolated from UiB2003 brains with astroglial DJ-1 expression on the other hand seemed to maintain its complex I activity.
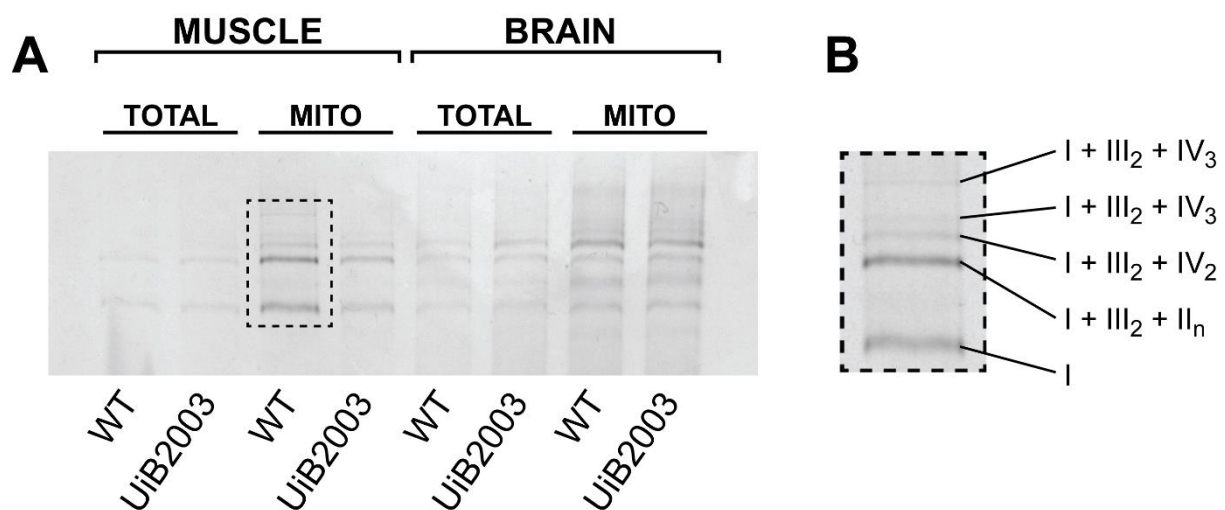
Fig. 4.8 Complex I activity in skeletal muscle and brain of WT and UiB2003 fish. A: Adult WT and UiB2003 (*park7$^{-/-}$,Tg(gfap:egfp-2A-flag-zDJ-1$_{C106A}$)*) fish were euthanised and brain and skeletal muscle were harvested. Muscle samples were collected from single fish while three brains per line were combined for the brain for further mitochondria isolation. Extract total lysates (TOTAL) and mitochondrial fraction lysates (MITO) were analysed by native PAGE followed and in-gel mitochondrial complex I activity assay. **B:** Supercomplex composition of complex I bands.

4.3 Intracellular localization of WT and mutant DJ-1 in oxidative-stressed cells

4.3.1 Verification of functional DJ-1-APEX2 expression in SH-SH5Y cells

The fusion protein plasmids, pcDNA3 Flag-DJ-1$_{WT}$-APEX2-NES and pcDNA3 Flag-DJ-1$_{C106A}$-APEX2-NES were verified by sequencing and used to transiently transfect SH-SY5Y cells. Cells were exposed for 24 h to 250 nM rotenone or vehicle starting the day after transfection. Cells were then fixed and stained with diaminobenzidine (DAB) (Fig. 4.9). DAB staining could be detected by low magnification (10x) light microscopy and was observed as light brown coloration in the cytoplasm. The transfection efficiency was ca. 20-30% in all transfected samples (panel A, B, C and D) regardless of DJ-1-APEX2 variant and treatment (data not shown). No staining was observed in the non-transfected DAB-stained control (Fig. 4.9 E).
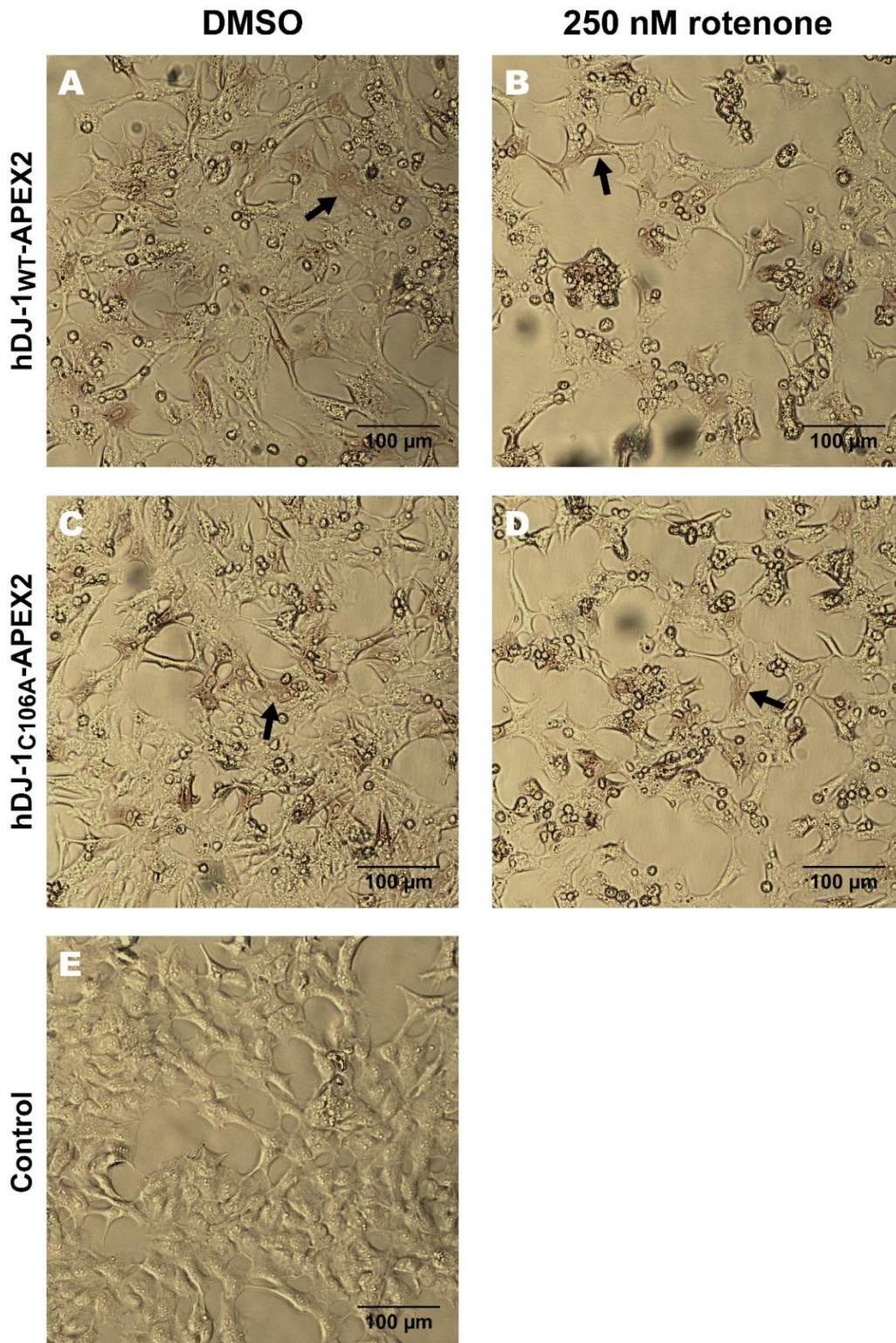
Fig. 4.9 Diaminobenzidine staining in transfected SH-SY5Y cells visualised by light microscopy SH-SY5Y cells were transfected with pcDNA3 hDJ-1$_{WT}$-APEX2-NES (panel A and B), pcDNA3 hDJ-1$_{C106A}$-APEX2-NES (panel C and D) or non-transfected as control (panel E), and after 24 h exposed to 250 nM rotenone (panel B and D) or to DMSO (panel A, C and E) for 24 hours before fixation and diaminobenzidine staining. DAB staining was visualised by light microscopy. Examples of DAB-stained cells are indicated in panel A, B, C and D by arrows. No DAB staining could be observed in the non-transfected control (panel E).

4.3.2 Ultrastructural determination of WT DJ-1 and mutant DJ-1 localization

There is conflicting evidence as to whether the cysteine in position 106 of DJ-1 is necessary for the mitochondrial localization of DJ-1 in response to oxidative stress or not (Canet-Aviles et al., 2004, Junn et al., 2009). The intramitochondrial localization of the DJ-1 has been proposed as outer membrane-restricted and conversely, matrix and inter-membrane space-only (Canet-Aviles et al., 2004, Junn et al., 2009, Zhang et al., 2005). In order to further investigate mitochondrial translocation of DJ-1 following exposure to oxidative stress, and the importance of C106 in this process, we wanted to determine the ultrastructural localization pattern of DJ-1 WT and a C106A mutant using APEX2-fusion proteins. Following detection of DAB staining by low magnification light microscopy (Fig. 4.9) SH-SY5Y cells were post-fixed, sectioned and stained for transmission electron microscopy and subsequently imaged (Fig 4.10). Transfected cells were easily detected by the increased TEM contrast caused by the DAB polymer and could be seen as dark colouration throughout the cytoplasm (Fig. 4.10 A, yellow frame). In non-transfected cells (Fig 4.10 A, orange frame) only the light background from osmium/uranyl staining was visible.

No difference in staining intensity in the mitochondrial intermembrane space or matrix between transfected (Fig. 4.10 B, yellow frame) and non-transfected (Fig. 4.10 B, orange frame) cells was observed. The outer membrane did, however, appear darker in transfected cells. Thus, DJ-1 and the mutant version seem not to be localized in the mitochondria, but possibly associated to the outer mitochondrial membrane.
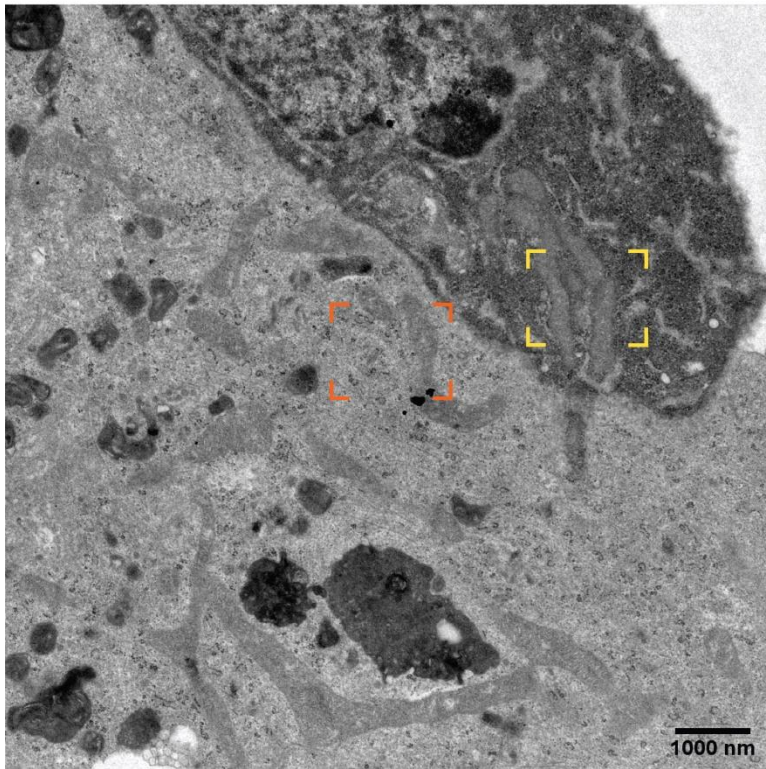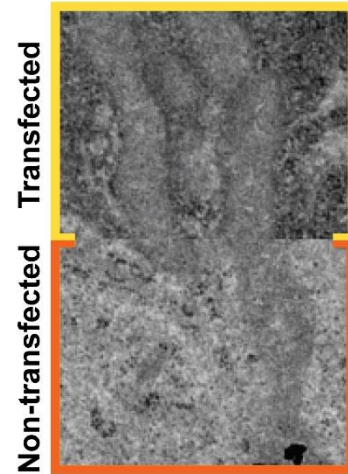
Fig. 4.10 Diaminobenzidine staining in transfected and non-transfected SH-SY5Y cells visualized by transmission electron microscopy SH-SY5Y cells were transfected with pcDNA3 hDJ-1$_{WT}$-APEX2-NES and on the following day exposed to 250 nM rotenone for 24 hours before fixation and diaminobenzidine staining. Samples were subsequently analysed by transmission electron microscopy. **A**: A transfected cell with pronounced DAB staining (yellow frame) is shown next to a non-transfected cell with no DAB staining (orange frame). The staining is prominent in the cytosol with unstained ER visible as white bands. **B**: A comparison of the mitochondria in the transfected cell in A (yellow border) with those of the non-transfected cell in A (orange border). The corresponding areas in A are indicated by a yellow and orange frame respectively. A scalebar (1000 nm) is indicated in A.

4.3.2 DJ-1 induced endoplasmic reticulum-mitochondria contact is unaffected by DJ-1 mutation at 106

The fusion protein plasmids, pcDNA3 Flag-DJ-1$_{WT}$-APEX2-NES and pcDNA3 Flag-DJ-1$_{C106A}$-APEX2-NES, were used to transiently transfect SH-SY5Y cells, and after 24 h the cells were treated with 250 nM rotenone or DMSO control. The cells were fixed after 24 h of rotenone/DMSO exposure, and subsequently stained with diaminobenzidine, and post-fixed, sectioned and stained for transmission electron microscopy (Fig. 4.11). Due to a lack of DAB polymerisation in the endoplasmic reticulum, the ER is clearly visible as light bands throughout the cytoplasm of transfected cells. An increase in ER-mitochondria contact was seen in all transfected samples (Fig. 4.11 A, B, C, D) with ER wrapped closely around the mitochondria on these samples. The same interaction was not seen in the non-transfected control (Fig. 4.11 E) or in unstained cells within any of the transfected samples (data not shown).

DMSO

250 nM rotenone

hDJ-1_{WT}-APEX2
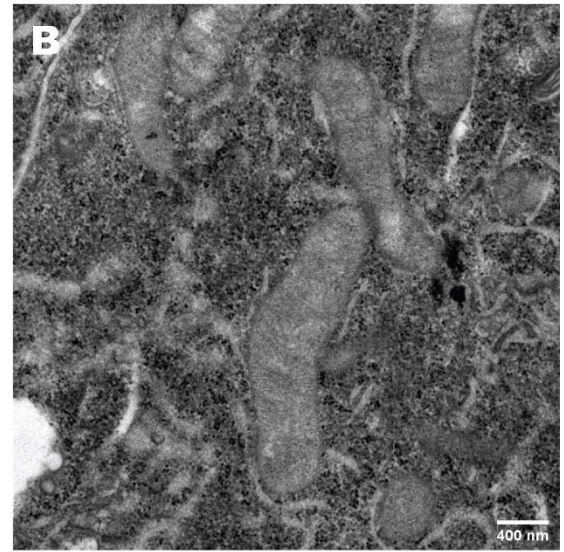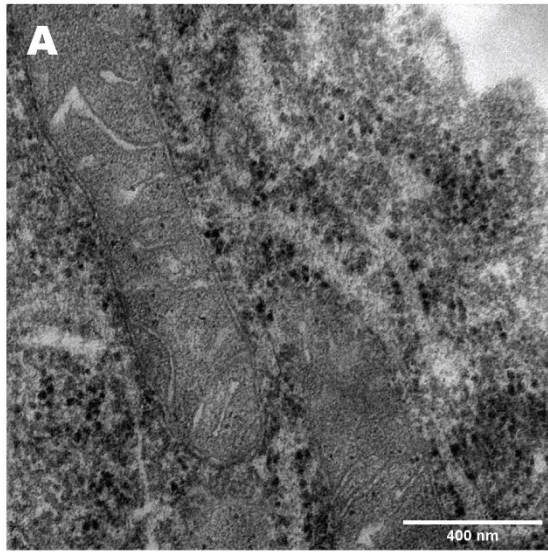
hDJ-1_{C106A}-APEX2

Control

A

B

C

D

E

400 nm
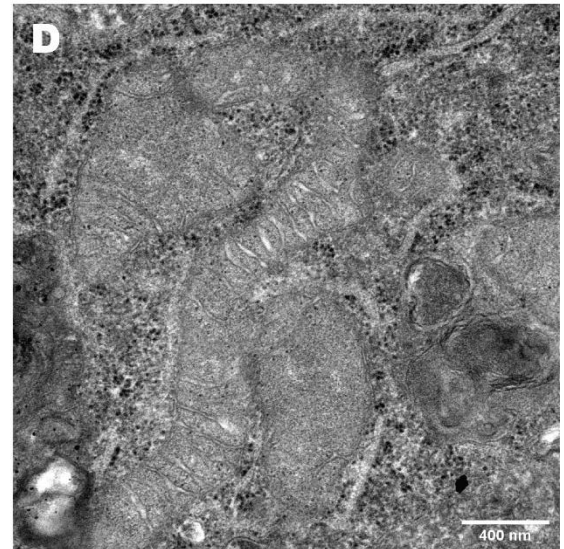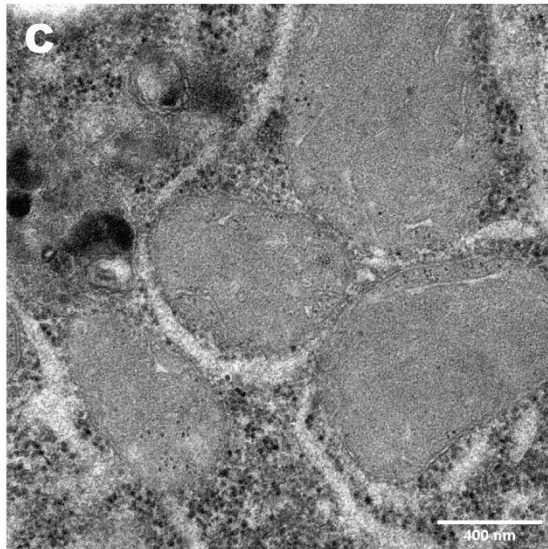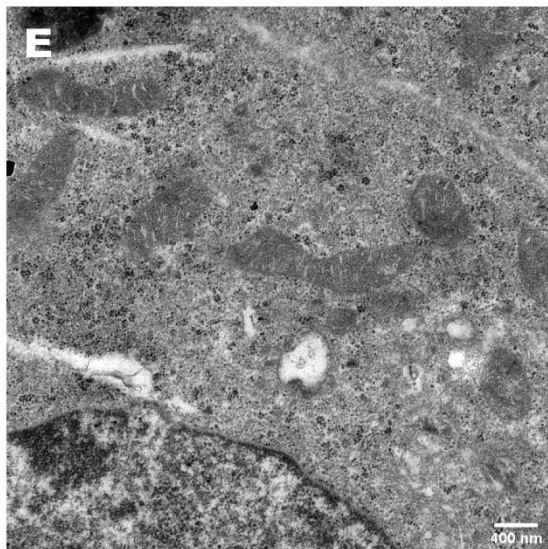
Fig. 4.11 Overexpression of DJ-1$_{WT}$ and DJ-1$_{C106A}$ increase contact between the endoplasmic reticulum and mitochondria. SH-SY5Y cells were transiently transfected with pcDNA3 Flag-DJ-1$_{WT}$-APEX2-NES (A-B) and pcDNA3 Flag-DJ-1$_{C106A}$-APEX2-NES (C-D) or non-transfected as a control (E). 24 hours after transfection cells were exposed to 250 nM rotenone (B and D) or DMSO as control (A, C and E) for 24 hours. Cells were then fixed, stained with diaminobenzidine and imaged by transmission electron microscopy. All transfected samples showed increased ER-mitochondria contact with ER appearing as white bands coiled around the mitochondria. This increased interaction was not seen in the non-transfected control sample (E) or in unstained cells within the transfected samples. A scale bar is indicated in each panel.

5 Discussion

Since the discovery of DJ-1s role in the cellular defence against oxidative stress and implication in both familial and sporadic forms of Parkinson's disease, much effort has been put into understanding the mechanisms and signalling pathways regulated by this protein. In this thesis we have examined the importance of the highly conserved and proposed oxidative sensor C106 residue of DJ-1.

5.1 Establishment and characterization of the UiB2003 line

By establishing the UiB2003 zebrafish line (*park7$^{-/-}$,Tg(gfap:egfp-2A-flag-zDJ-1$_{C106A}$)*) and comparing it to wild type, and the established DJ-1 KO *(park7$^{-/-}$)* and UiB2001 line (*park7$^{-/-}$,Tg(gfap:egfp-2A-flag-zDJ-1)*), we wanted to examine the oxidative stress-mitigating ability of DJ-1 and the impact of a C106A mutation on this protective function *in vivo*.

The expression pattern of DJ-1$_{C106A}$ in the UiB2003 line was determined by the reporter protein eGFP. The insert that is cut out by I-SceI and integrated into the zebrafish genome consists of the gene for eGFP and Flag-DJ-1$_{C106A}$ linked by a viral 2A segment. The function of this 2A segment is to prevent eGFP from interfering with the activity of DJ-1$_{C106A}$, as might be the case with fused proteins. The 2A viral peptide mediates formation of two separate protein from a single transcribed mRNA when it is positioned between two genes (Kim et al., 2011). The two proteins are expressed in equimolar amounts as two separate proteins. The successful breaking of 2A is easily demonstrated by the fact that Western blots of UiB2003 lysates probed for DJ-1 (Fig. 4.3) showed the DJ-1$_{C106A}$ band at the expected size of 22 kDa, and not 49 kDa as would have been expected of the fused proteins.

Because both eGFP and DJ-1$_{C106A}$ are transcribed simultaneously under the regulation of the same *gfap* regulatory elements, the expression of eGFP is assumed to correspond to the expression pattern of DJ-1$_{C106A}$. The cellular expression pattern was determined by fluorescence microscopy (Fig. 4.2). At 1 dpf positive embryos displayed eGFP expression in the head region and along the developing spinal cord. At 2dpf the expression was more distinct, appearing in the brain, retina and along the spine of positive larvae. This expression pattern coincides well the observations of Bernados and Raymond (Bernardos and Raymond, 2006). They used the same GFAP-derived regulatory elements to generate a transgenic zebrafish line with glial expression of green fluorescent protein (GFP), *Tg(gfap:GFP)*. At 24 hpf they observed GFP-expressing cells from the developing brain and along the developing spinal cord, but also in the retina and lens of the embryos. At 72 hpf prominent GFP expression was observed in the glial

cells of the brain, neural retina, spinal cord and ventral spinal nerves. Our group has previously demonstrated gfap reporter driven constructs to be astroglial specific in the zebrafish brain (Froyset et al., 2018).

5.1.1 Transgene inheritance in the UiB2003 line

The astroglial-restricted DJ-1$_{C106A}$ line, UiB2003, was established using I-SceI meganuclease-based transgenesis. The resulting F0 fish demonstrated a broad range of germline transmission, with 1-50% positive progeny depending on the parent fish outcrossed. This indicates a certain degree of mosaicism at the F0 generation, as is expected of the I-SceI system. The germline transmission rate cut-off at 50% indicates single insertion events of the transgene and is further supported by the Mendelian distribution of the transgene observed at both the F1 generation and F2 generation. This is expected as I-SceI-based transgenesis has been shown to favour insertion at a single locus. It should be noted that although I-SceI generally leads to a single insertion event, this does not guarantee insertion of a single copy of the transgene. It has been demonstrated that 1-10 copies in tandem repeat are generally inserted (Grabher et al., 2004). Furthermore, as the site of insertion is nonspecific, each F0 fish will have the transgene inserted at a different location in the genome, which can in turn affect expression levels further. This could partly explain the degree of variation between individuals observed, as individuals could have different copy numbers that affects the level of expression and thus their response to experimental treatment. Additionally, the UiB2003 F1 generation was not based on a single F0 founder fish but consists of the combined offspring of multiple outcrossed founders. This is expected to result in higher variance than using a single founder fish.

5.1.2 DJ-1 expression levels in transgenic zebrafish

The expression level of the DJ-1$_{C106A}$ in the UiB2003 line is more than 10 times higher than endogenous DJ-1 levels in astroglia. This is based on the observation that the flag-tagged DJ-1$_{C106A}$ had higher expression than what was seen for the flag-tagged DJ-1$_{WT}$ of the UiB1001 line (Fig. 4.3). The astroglial-targeted flag-DJ-1$_{WT}$ of the UiB1001 line is known to be expressed at about 10 times the level of the endogenous astroglial DJ-1 (Froyset et al., 2018). Due to being under the control of not the natural regulative elements of DJ-1 but those of GFAP, the level of expression will be different from endogenous DJ-1. As for the difference in expression level between DJ-1$_{C106A}$ in UiB2003 and flag-DJ-1$_{WT}$ of the UiB1001 line, this may be due to the mechanism of I-SceI-based transgenesis. While I-SceI generally favours single insertion events, it can lead to insertion of low copy number tandem repeats of the gene to be inserted (Thermes et al., 2002). A difference in copy number between the two lines may result

in different expression levels. Additionally, because the site of insertion is random, the location of the transgene and thus the genomic environment will differ between the lines and between individuals, further affecting expression levels (Liu, 2013). The high expression level in the UiB2003 line could affect the activity of DJ-1$_{C106A}$, as this may promote interactions that would not occur at endogenous concentrations under basal conditions. It should however be noted that DJ-1 has been found to be upregulated in the astrocytes of sporadic PD patients (Bandopadhyay et al., 2004). Thus, astrocytic overexpression of DJ-1 may be used to model this PD-characteristic expression.

5.1.2 Astroglial-restricted overexpression of DJ-1$_{C106A}$ is non-lethal and without phenotype in larvae and young adult zebrafish

No distinct effect on egg quality or number, development, larval survival or fertility were observed in the UiB2003 line under basal conditions. This reflects what has previously been observed for the DJ-1 KO line, which does not exhibit a phenotype at this stage (Edson et al., 2019). An age-related parkinsonian phenotype has however been observed in the DJ-1 KO fish aged 1.5-2 years. At this age, some fish may develop a distinct phenotype of low body weight and decreased pigmentation. This phenotype is also more common in male fish, possibly reflecting the higher tendency of men to develop PD seen in humans (Miller and Cronin-Golomb, 2010). Neither the UiB2003 line nor the corresponding UiB2001 line have yet reached the age where this phenotype occurs in the DJ-1 KO fish. It is therefore still unknown whether these lines will develop the same sex-linked phenotype. Either outcome will yield further insight into the impact of astroglial-restricted DJ-1 expression as well as the C106A mutation. Due to the mosaicism in the F0 generation, any conclusions on the phenotype should not be drawn from this generation, as the effect may be due to the fish being partly KO. Any conclusions regarding phenotype should initially be made from the heterozygous F1 generation where the gene is ubiquitous throughout the body and astroglial expression is uniform. Conclusions from the F1 generation could be further validated with comparison to future homozygous F2 generations, in case the expression level of DJ-1 plays a role.

5.1.3 Effect of rotenone-induced oxidative stress on gross larval anatomy

In the event that the C106A mutation renders DJ-1 completely non-functional, one might have expected to see the UiB2003 line respond to oxidative stress in a similar manner as the DJ-1 KO line. This however, as evident by the results of the rotenone experiments (Fig. 4.5, Fig. 4.6 and Fig. 4.7) was not the case. Surprisingly, the UiB2003 line performed consistently worse than the DJ-1 KO line in its ability to withstand oxidative stress, as shown in the rotenone

experiments (Fig. 4.5). After exposure to rotenone, UiB2003 larvae displayed a significantly lower survival rate than both WT and DJ-1 KO larvae, averaging at about 50%, while the survival of WT and DJ-1 KO larvae was largely unaffected. Similarly, the propensity to develop edema was far higher in treated UiB2003 larvae. As for the rotenone-induced lowering of heart rate, this was more severe in UiB2003 compared to the DJ-1 KO. The rotenone dose-response experiment also demonstrated a higher sensitivity to rotenone in the UiB2003 line, with the entire group having developed edema at the lowest concentration where WT and DJ-1 KO larvae appeared completely unaffected (Fig. 4.7). One possible explanation is that DJ-1$_{C106A}$ is dysfunctional and unable to exert its protective function, but at the same time perceived by the cellular machinery as a functional defence already in action, thereby downregulating or delaying alternative protective pathways. In the DJ-1 KO line, no DJ-1 is present and any defence must come immediately from the alternative protective pathways leading to faster response.

Interestingly, an effect similar to that seen for UiB2003 was seen in the UiB2001 line. When treated with rotenone these larvae had significantly lower survival rate than both the corresponding WT and DJ-1 KO group. This may indicate that the lack of protection against oxidative stress in astroglial-restricted DJ-1 larvae is independent of the C106 residue. Based on the finding that astroglial overexpression of DJ-1$_{WT}$ in the UiB1001 is protective compared to endogenous DJ-1 only (Froyset et al., 2018), we initially hypothesised that astroglial overexpression of DJ-1$_{WT}$ in larvae with no endogenous DJ-1 could confer some protective effect compared to larvae lacking DJ-1 entirely. This is not supported by the findings of this thesis. The high astroglial DJ-1$_{WT}$ level may be sufficient to hinder other protective pathways, while at the same time unable to compensate for the lack of endogenous DJ-1 throughout the body. This is one of the major difficulties when working with living systems, upregulating a single protein can be expected to have a particular effect based on the known pathways it is involved in, but may still produce seemingly contradictory results because the complete effects of the biological context are not known.

5.1.4 UiB2003 larvae have altered protein expression both under basal conditions and during rotenone-induced oxidative stress

Following the assessment of gross anatomy and heart rate in response to rotenone-induced oxidative stress in the zebrafish larvae. Whole larvae protein lysates were prepared from the larvae and analysed thorough Western blotting.

Analysis of the expression of tyrosine hydroxylase, a marker for dopaminergic cells, in whole larvae lysates showed a markedly lower ($p<0.01$) level in rotenone-treated WT larvae compared to WT control larvae (Fig. 4.6). This was expected as rotenone, as well as other parkinsonian phenotype-inducing neurotoxicants, have been shown to cause a reduction in TH levels or TH-positive cells both *in vitro* and *in vivo* (Luo et al., 2007, Marella et al., 2009, Zagoura et al., 2017). Notably, a similar reduction in TH expression of WT zebrafish larvae has been shown in our lab previously using MPP^+ (Froyset et al., 2018). In the current study none of the lines aside from the WT showed a significant difference in TH levels between treated and untreated larvae. One interesting result however, was the markedly lower ($p<0.05$) TH level found in untreated UiB2003 larvae compared to untreated WT. This is in stark contrast to the protective effect that has previously been observed with the astroglial DJ-1$_{WT}$ overexpression line, UiB1001 (Froyset et al., 2018). Due to the high variation and small sample size of the UiB2001 larvae groups, which expresses the astroglial-restricted DJ-1$_{WT}$, it cannot be determined if this effect seen in UiB2003 larvae is due to the C106A mutation or if it is related to the fact that expression is restricted to astroglia. There were some problems with obtaining eggs from the UiB2001 fish, for the experiments, so this should ideally be repeated with larger experimental groups. It may be interesting to see if the low TH level in the UiB2003 line under basal conditions is specific to the larvae or if this is something that can be observed in the adult fish as well. Nevertheless, this seemingly disadvantageous effect of astroglial DJ-1$_{C106A}$ even under basal conditions, further supports what was seen for survival, edema and heart rate, that astroglial DJ-1$_{C106A}$ has a net negative effect.

In addition to tyrosine hydroxylase, the effect of rotenone-induced oxidative stress on the expression of inducible nitric oxide synthase (iNOS), a marker of intracellular stress, was also assessed. Here elevated iNOS levels were observed in rotenone-treated DJ-1 KO larvae compared to the treated WT larvae ($p<0.05$), while the rotenone-treated UiB2003 larvae on the other hand expressed significantly less iNOS than the DJ-1 KO ($p<0.05$). This could indicate a protective effect of the astroglial DJ-1$_{C106A}$ despite the mutation. DJ-1 is known to act as a negative regulator of iNOS, supressing iNOS induction under conditions of oxidative stress (Waak et al., 2009) (see Fig. 1.3). This could explain the significantly higher level of iNOS observed in the rotenone-treated DJ-1 KO larvae compared to the wild type. With no DJ-1 present, the induction of iNOS is not halted through this pathway. Following this, the observation that the UiB2003 larvae show significantly lower expression of iNOS could lead one to believe that DJ-1$_{C106A}$ simply acts to inhibit iNOS induction the same way DJ-1$_{WT}$ does.

A counterargument to this idea, however, is the mechanism of iNOS inhibition. This regulation is reportedly mediated via direct binding to ASK1, thereby preventing the activating signalling pathway from ASK1 via p38/MAPK to iNOS. This binding has been shown to be dependent on disulphide-bonding via C106 in DJ-1 and is abolished in DJ-1$_{C106A}$. The effect on iNOS seen in UiB2003 larvae may therefore not be due to the standard inhibition of iNOS induction.

5.1.5 Mitochondrial complex I activity in the brain, but not in skeletal muscle, is rescued by astroglial expression of DJ-1$_{C106A}$

Complex I dysregulation has been linked to the pathogenesis of PD, as both the activity and amount of complex I has been found to be reduced in post-mortem *substantia nigra* of PD patients (Schapira et al., 1990).

Previous results from studying the DJ-1 KO zebrafish line in our lab have shown a DJ-1 dependent effect on both the expression level of mitochondrial complex I components and on the activity of the complex (Edson et al., 2019). A complex I activity assay performed using protein lysates from WT and DJ-1 KO adult fish showed reduced complex I activity in the DJ-1 KO both in skeletal muscle (Edson et al., 2019) and in brain compared to the WT reference (Elda, unpublished data). We then wanted to investigate if astroglial DJ-1$_{C106A}$ in UiB2003 fish would rescue this drop in complex I activity. While DJ-1 has been shown to be involved in the regulation of mitochondrial complex I activity, little is known about the role of cysteine 106 in this regulation (Hayashi et al., 2009). By comparing samples of astroglia-rich brain with skeletal muscle, which does not contain astroglia, the effect of DJ-1$_{C106A}$ vas examined. As seen in figure 4.8, the C106A mutant form of DJ-1 appears to retain some of its function. Complex I activity remained unaffected compared to WT in brain samples but was reduced in skeletal muscle tissue. This tissue-specific effect is likely due to the lack of astroglia in skeletal muscle and high number in brain. Thus, C106 does not appear to be critical for the complex I-regulating activity of DJ-1.

5.2 hDJ-1$_{WT/C106A}$-APEX2 fusion protein-based protein localization

The C106 residue has been proposed to be an oxidative stress sensor which upon oxidation enables DJ-1 to translocate to the mitochondria (Junn et al., 2009, Canet-Aviles et al., 2004). Conflicting results have been shown as to where DJ-1 localizes in the mitochondria and to what degree the C106 is involved (Canet-Aviles et al., 2004, Junn et al., 2009, Cali et al., 2015). To further investigate the role of C106 we utilized the newly developed APEX2-based method which in combination with transmission electron microscopy (TEM) and mass spectrometry

can be used to determine intracellular localization and protein-protein interaction (Lam et al., 2015, Martell et al., 2017, Hung et al., 2016).

5.2.1 Considerations for the fusion of APEX2 to DJ-1

One major point of concern when designing the DJ-1$_{WT/C106A}$-APEX2 constructs was the possibility of APEX2-fusion to DJ-1 altering the activity of DJ-1. DJ-1 is a relatively small protein at only ca. 20 kDa. Linking it to APEX2, a 27 kDa protein could therefore perturb its endogenous function and localization. This is one of the main concerns with using the APEX2 method for ultrastructural localization.

It has been proposed that the N-terminal sequence of DJ-1 is needed for the protein to translocate to the mitochondria (Maita et al., 2013). The attachment of an N-terminal Flag tag or the deletion of the N-terminal most 12 amino acids led to altered localization of both wild type and some mutant forms of DJ-1, to mainly cytosolic. The change in wild type DJ-1 localization was not dramatic. It should, however, be noted that this was under basal conditions and not under elevated oxidative stress. Due to the possible involvement of the N-terminal end in localization, we decided to fuse APEX2 to the C-terminal ends of DJ-1$_{WT}$ and DJ-1$_{C106A}$ respectively.

One particular concern was whether APEX2-linking would interfere with DJ-1 dimerization. The importance of dimerization for DJ-1 to exert its functions has been demonstrated by mutant forms of the protein. One of the first two DJ-1 mutations found to cause familial PD, the loss-of function L166P mutation, was later discovered to impair the formation of DJ-1 homodimers, as did multiple other PD causative mutations (M26I, L10P, and P158Δ) (Repici et al., 2013). It is therefore believed that formation of homodimers is integral in the normal function of DJ-1 and that inability to dimerize is the main reason these mutations are detrimental. Both termini of APEX2 are positioned at the surface of the protein and based on crystal structures, the C-terminal ends of DJ-1 appear to protrude from the surface of the DJ-1 dimer as well. To reduce the risk of steric interference, DJ-1 and APEX2 were not fused directly but connected by a flexible linker region. Furthermore, it has previously been shown in our lab that fusing DJ-1 to green fluorescent protein does not prevent dimerization of DJ-1 (Fladmark, unpublished data). As GFP and APEX2 are the same size and both have globular shapes, this would suggest that the DJ-1 dimer should be able to form despite fusion to APEX2 (Martell et al., 2017).

5.2.2 Ultrastructural localization of APEX2-fused DJ-1 WT and mutant form

The cellular localization of DJ-1 was initially determined by fractionation and fluorescence analysis of EGFP-linked DJ-1 and found to be largely cytoplasmic with a smaller pool of DJ-1 inhabiting the nucleus (Nagakubo et al., 1997). Since then, multiple studies have proposed a mitochondria-localized pool of DJ-1 as well, possibly dependent on the oxidative state of the cell. This is however disputed. One study found endogenous DJ-1 in mouse cell cultures to not colocalize with mitochondrial marker under basal conditions at all (Bandopadhyay et al., 2004). Conversely, Zhang et al. found 25% of DJ-1 to localize to the mitochondria in SH-SY5Y cells based on subcellular fractionation, independent of treatment with a PD model neurotoxicant (paraquat) (Zhang et al., 2005). Yet another study, based on a split-GPF-based approach, found the translocation of DJ-1$_{WT}$ to be dependent on oxidative stress induced by rotenone or H_2O_2, or on nutrient depletion, and a C106T mutant unable to translocate (Cali et al., 2015). Junn et al. found 8-10% of DJ-1$_{WT}$ and DJ-1$_{C106S}$ to translocate to the mitochondria, but only following exposure to oxidative stress (H_2O_2), suggesting that oxidative stress, but not cysteine 106, is essential for translocation (Junn et al., 2009). Canet-Avilés et al, on the other hand, while also deeming oxidative stress essential for translocation, found the C106 to be essential and translocation to be abrogated in DJ-1$_{C106A}$. Opinions on the sub-mitochondrial localization of DJ-1 is also conflicting, with outer membrane (OMM)-only, inter membrane space and matrix-restricted, or matrix has been proposed (Canet-Aviles et al., 2004, Junn et al., 2009, Cali et al., 2015).

At the high mitochondrial DJ-1 levels proposed by Zhang et al. and Junn et al. (Junn et al., 2009, Zhang et al., 2005), mitochondrial DJ-1 staining, and particularly interior staining, should be easily identified in the TEM images using the APEX2-based method, but no such strong staining is observed when transfecting our APEX2 constructs into the neuroblastoma cell line SH-SY5Y (Fig. 4.10). There was no observable localization to the mitochondrial inter-membrane space or matrix in rotenone-treated SH-SY5Y cells expressing DJ-1$_{WT}$-APEX2. Possibly some stronger staining on the outer mitochondrial membrane compared to the inner membrane could be seen, but to determine this would require a more thorough densiometric analysis across the mitochondrial membranes, and preferably by comparing the OMM to MIM staining intensity ratio of APEX2-DJ-1-transfected cells with the ratio in APEX2-NES-transfected cells, as this would provide a more similar cytosolic background stain.

As stated in section 5.2.1, there is of course the possibility of APEX2 fusion interfering with DJ-1s ability to translocate to the mitochondria. One study found the monomeric form of DJ-1

mutants to readily translocate to the mitochondria, but whether the monomeric form is needed for translocation to occur with DJ-1$_{WT}$ is not known (Maita et al., 2013). If the monomeric form is needed due to a size constraint in the process facilitating transport across the OMM and/or MIM, fusion with APEX2 would likely interfere.

5.2.3 DJ-1 and effect on ER-mitochondria association

During the TEM-based visualisation of DJ-1 localization, we noticed a change in the organisation of organelles in transfected vs. non-transfected cells. APEX2-DJ-1-overexpressing cells displayed a pronounced increase in the contact between the mitochondria and endoplasmic reticulum (Fig. 4.11). This effect of APEX2-DJ-1 overexpression was independent both of C106 and rotenone induced oxidative stress.

Dysregulation of mitochondrial function has long been implicated in neurodegenerative disorders. More recently, attention has been brought to the role of mitochondria-associated ER membranes (MAMs), specialised ER subdomains that act as contact sites linking the ER and mitochondrial networks. MAMs have several functions including lipid synthesis, calcium signalling and uptake in the mitochondria, bioenergetics, and apoptosis, and there is now emerging evidence that dysregulation of these MAMs play a role in neurodegenerative disorders, including Parkinson's disease (Liu and Zhu, 2017, Paillusson et al., 2016). Overexpression of DJ-1 has previously been shown to promote an increase in the contact between endoplasmic reticulum and mitochondria, indicating a regulatory role in MAMs (Ottolini et al., 2013). Thus, our study supports this and does also suggest that the effect on MAMs is not C106 dependent.

6 Conclusions

Astroglial-restricted expression of DJ-1$_{C106A}$ does not protect zebrafish larvae from rotenone-induced insult and in fact proved more detrimental than a complete lack of DJ-1, with lower survival, high edema incidence and lowered heartrate, as well as higher sensitivity to low doses of rotenone. At the protein level, astroglial-restricted expression of DJ-1$_{C106A}$ led to altered iNOS and TH expression compared to that seen in WT and DJ-1 KO groups, both under basal conditions and during oxidative stress.

DJ-1 does not appear to enter the intermembrane space or matrix of mitochondria in SH-SY5Y cells, independent of cysteine 106 and exposure to oxidative stress. Localization to the outer mitochondrial membrane is a possibility but requires further investigation. Overexpression of DJ-1 was however found to induce increased ER-mitochondria contact in a C106 independent manner.

DJ-1$_{C106A}$ appears to be partly functional, retaining some activities that are lost in KO systems such as regulation of mitochondrial complex I and suppression of iNOS induction in zebrafish larvae.

7 Future perspectives

As previously mentioned in section 5.1.2, the DJ-1 KO fish have been shown to develop an age-related parkinsonian phenotype, where the fish, and especially the males, have lower body weight and become pale at 1.5-2 years of age. It would be interesting to see in the future whether UiB2001 and UiB2003 fish develop a similar phenotype.

The UiB2001 and UiB2003 lines provide a means to further examine the effect of DJ-1 overexpression on the astroglial protein profile of zebrafish, free of the endogenous background. This may lead to greater insight into the role of the C106 residue, as the lines can be compared and differences in protein regulation determined. This could also validate the results found for DJ-1's effect on complex I activity in the adult zebrafish, as you could determine if the upregulation of complex I components seen in the DJ-1 KO line (Edson et al., 2019) is missing in the UiB2001 and UiB2003 lines. Considering that both UiB2001 and UiB2003 fish have astroglial-restricted expression of eGFP, one could do FACS-based cell sorting followed by astroglial-specific protein mapping to identify effects of C106 on the astroglial proteome.

The effect of on mitochondrial functions such as complex I activity may be further examined by Seahorse XF-based metabolic studies, either on whole larvae or on extracted mitochondria.

The protective function of DJ-1 is proposed to act via the Nrf2/ARE pathway and to be dependent on functional DJ-1 C106 oxidation (Edson et al., 2019, Moscovitz et al., 2015). We have newly obtained a Nrf2 activity reporter construct that could be used in combination with the UiB2001 and UiB2003 lines to examine the involvement of Nrf2 activation. If there is a C106-dependent difference in Nrf2 activation in response to oxidative stress, this could be quantified. Is the reduced protection from rotenone-induced insult, that was observed in the UiB2003 line, due to impaired Nrf2 activation?

We were not able to determine whether DJ-1 localizes with the OMM, as has been proposed in multiple studies. One way to further examine this would be to determine localization using APEX2-NES-expressing cells as reference. This could make densiometric analysis of DAB staining across the mitochondrial outer and inner membrane easier, as it would give a similar background staining. There was a possible difference in staining intensity of the outer and inner mitochondrial membrane of transfected cells, but this proved difficult to quantify due to the high cytoplasmic background staining.

Proximity-based protein mapping (see section 1.6) with the APEX2 constructs could be used to compare the DJ-1$_{WT}$ and the DJ-1$_{C106A}$ interactome, and especially proteins linked to oxidative stress response and the Nrf2 pathway.

8 References

ANDRES-MATEOS, E., PERIER, C., ZHANG, L., BLANCHARD-FILLION, B., GRECO, T. M., THOMAS, B., KO, H. S., SASAKI, M., ISCHIROPOULOS, H., PRZEDBORSKI, S., DAWSON, T. M. & DAWSON, V. L. 2007. DJ-1 gene deletion reveals that DJ-1 is an atypical peroxiredoxin-like peroxidase. *Proc Natl Acad Sci U S A,* 104**,** 14807-12.

ARIGA, H., TAKAHASHI-NIKI, K., KATO, I., MAITA, H., NIKI, T. & IGUCHI-ARIGA, S. M. 2013. Neuroprotective function of DJ-1 in Parkinson's disease. *Oxid Med Cell Longev,* 2013**,** 683920.

BANDOPADHYAY, R., KINGSBURY, A. E., COOKSON, M. R., REID, A. R., EVANS, I. M., HOPE, A. D., PITTMAN, A. M., LASHLEY, T., CANET-AVILES, R., MILLER, D. W., MCLENDON, C., STRAND, C., LEONARD, A. J., ABOU-SLEIMAN, P. M., HEALY, D. G., ARIGA, H., WOOD, N. W., DE SILVA, R., REVESZ, T., HARDY, J. A. & LEES, A. J. 2004. The expression of DJ-1 (PARK7) in normal human CNS and idiopathic Parkinson's disease. *Brain,* 127**,** 420-430.

BERNARDOS, R. L. & RAYMOND, P. A. 2006. GFAP transgenic zebrafish. *Gene Expr Patterns,* 6**,** 1007-13.

BEST, J. D. & ALDERTON, W. K. 2008. Zebrafish: An in vivo model for the study of neurological diseases. *Neuropsychiatr Dis Treat,* 4**,** 567-76.

BLACKINTON, J., LAKSHMINARASIMHAN, M., THOMAS, K. J., AHMAD, R., GREGGIO, E., RAZA, A. S., COOKSON, M. R. & WILSON, M. A. 2009. Formation of a stabilized cysteine sulfinic acid is critical for the mitochondrial function of the parkinsonism protein DJ-1. *J Biol Chem,* 284**,** 6476-85.

BONIFATI, V., RIZZU, P., VAN BAREN, M. J., SCHAAP, O., BREEDVELD, G. J., KRIEGER, E., DEKKER, M. C., SQUITIERI, F., IBANEZ, P., JOOSSE, M., VAN DONGEN, J. W., VANACORE, N., VAN SWIETEN, J. C., BRICE, A., MECO, G., VAN DUIJN, C. M., OOSTRA, B. A. & HEUTINK, P. 2003. Mutations in the DJ-1 gene associated with autosomal recessive early-onset parkinsonism. *Science,* 299**,** 256-9.

CALI, T., OTTOLINI, D., SORIANO, M. E. & BRINI, M. 2015. A new split-GFP-based probe reveals DJ-1 translocation into the mitochondrial matrix to sustain ATP synthesis upon nutrient deprivation. *Hum Mol Genet,* 24**,** 1045-60.

CANET-AVILES, R. M., WILSON, M. A., MILLER, D. W., AHMAD, R., MCLENDON, C., BANDYOPADHYAY, S., BAPTISTA, M. J., RINGE, D., PETSKO, G. A. & COOKSON, M. R. 2004. The Parkinson's disease protein DJ-1 is neuroprotective due to cysteine-sulfinic acid-driven mitochondrial localization. *Proc Natl Acad Sci U S A,* 101**,** 9103-8.

CHOI, J., SULLARDS, M. C., OLZMANN, J. A., REES, H. D., WEINTRAUB, S. T., BOSTWICK, D. E., GEARING, M., LEVEY, A. I., CHIN, L. S. & LI, L. 2006. Oxidative damage of DJ-1 is linked to sporadic Parkinson and Alzheimer diseases. *J Biol Chem,* 281**,** 10816-24.

CHOI, M. S., NAKAMURA, T., CHO, S. J., HAN, X., HOLLAND, E. A., QU, J., PETSKO, G. A., YATES, J. R., 3RD, LIDDINGTON, R. C. & LIPTON, S. A. 2014. Transnitrosylation from DJ-1 to PTEN attenuates neuronal cell death in parkinson's disease models. *J Neurosci,* 34**,** 15123-31.

CLEMENTS, C. M., MCNALLY, R. S., CONTI, B. J., MAK, T. W. & TING, J. P. 2006. DJ-1, a cancer- and Parkinson's disease-associated protein, stabilizes the antioxidant transcriptional master regulator Nrf2. *Proc Natl Acad Sci U S A,* 103**,** 15091-6.

DAWSON, T. M. & DAWSON, V. L. 2003. Rare genetic mutations shed light on the pathogenesis of Parkinson disease. *J Clin Invest,* 111**,** 145-51.

DE LAU, L. M. & BRETELER, M. M. 2006. Epidemiology of Parkinson's disease. *Lancet Neurol,* 5**,** 525-35.

DIAS, V., JUNN, E. & MOURADIAN, M. M. 2013. The role of oxidative stress in Parkinson's disease. *J Parkinsons Dis,* 3**,** 461-91.

EDSON, A. J., HUSHAGEN, H. A., FRØYSET, A., KHAN, E., DI STEFANO, A. & FLADMARK, K. E. 2019. Dysregulation in the brain protein profile of zebrafish lacking the Parkinson's disease related protein DJ-1. *Molecular Neurobiology*.

ESPINOSA-DIEZ, C., MIGUEL, V., MENNERICH, D., KIETZMANN, T., SANCHEZ-PEREZ, P., CADENAS, S. & LAMAS, S. 2015. Antioxidant responses and cellular adjustments to oxidative stress. *Redox Biol,* 6**,** 183-197.

FROYSET, A. K., EDSON, A. J., GHARBI, N., KHAN, E. A., DONDORP, D., BAI, Q., TIRABOSCHI, E., SUSTER, M. L., CONNOLLY, J. B., BURTON, E. A. & FLADMARK, K. E. 2018. Astroglial DJ-1 over-expression up-regulates proteins involved in redox regulation and is neuroprotective in vivo. *Redox Biol,* 16**,** 237-247.

GRABHER, C., JOLY, J.-S. & WITTBRODT, J. 2004. *Highly Efficient Zebrafish Transgenesis Mediated by the Meganuclease I-SceI*.

GREENAMYRE, J. T. & HASTINGS, T. G. 2004. Biomedicine. Parkinson's--divergent causes, convergent mechanisms. *Science,* 304**,** 1120-2.

GRUNWALD, D. J. & EISEN, J. S. 2002. Headwaters of the zebrafish -- emergence of a new model vertebrate. *Nat Rev Genet,* 3**,** 717-24.

HABAS, A., HAHN, J., WANG, X. & MARGETA, M. 2013. Neuronal activity regulates astrocytic Nrf2 signaling. *Proc Natl Acad Sci U S A,* 110**,** 18291-6.

HAO, L. Y., GIASSON, B. I. & BONINI, N. M. 2010. DJ-1 is critical for mitochondrial function and rescues PINK1 loss of function. *Proc Natl Acad Sci U S A,* 107**,** 9747-52.

HAYASHI, T., ISHIMORI, C., TAKAHASHI-NIKI, K., TAIRA, T., KIM, Y. C., MAITA, H., MAITA, C., ARIGA, H. & IGUCHI-ARIGA, S. M. 2009. DJ-1 binds to mitochondrial complex I and maintains its activity. *Biochem Biophys Res Commun,* 390**,** 667-72.

HEINZ, S., FREYBERGER, A., LAWRENZ, B., SCHLADT, L., SCHMUCK, G. & ELLINGER-ZIEGELBAUER, H. 2017. Mechanistic Investigations of the Mitochondrial Complex I Inhibitor Rotenone in the Context of Pharmacological and Safety Evaluation. *Sci Rep,* 7**,** 45465.

HEO, J. Y., PARK, J. H., KIM, S. J., SEO, K. S., HAN, J. S., LEE, S. H., KIM, J. M., PARK, J. I., PARK, S. K., LIM, K., HWANG, B. D., SHONG, M. & KWEON, G. R. 2012. DJ-1 null dopaminergic neuronal cells exhibit defects in mitochondrial function and structure: involvement of mitochondrial complex I assembly. *PLoS One,* 7**,** e32629.

HOLZSCHUH, J., RYU, S., ABERGER, F. & DRIEVER, W. 2001. Dopamine transporter expression distinguishes dopaminergic neurons from other catecholaminergic neurons in the developing zebrafish embryo. *Mech Dev,* 101**,** 237-43.

HONBOU, K., SUZUKI, N. N., HORIUCHI, M., NIKI, T., TAIRA, T., ARIGA, H. & INAGAKI, F. 2003. The crystal structure of DJ-1, a protein related to male fertility and Parkinson's disease. *J Biol Chem,* 278**,** 31380-4.

HOWE, K., CLARK, M. D., TORROJA, C. F., TORRANCE, J., BERTHELOT, C., MUFFATO, M., COLLINS, J. E., HUMPHRAY, S., MCLAREN, K., MATTHEWS, L., MCLAREN, S., SEALY, I., CACCAMO, M., CHURCHER, C., SCOTT, C., BARRETT, J. C., KOCH, R., RAUCH, G. J., WHITE, S., CHOW, W., KILIAN, B., QUINTAIS, L. T., GUERRA-ASSUNCAO, J. A., ZHOU, Y., GU, Y., YEN, J., VOGEL, J. H., EYRE, T., REDMOND, S., BANERJEE, R., CHI, J., FU, B., LANGLEY, E., MAGUIRE, S. F., LAIRD, G. K., LLOYD, D., KENYON, E., DONALDSON, S., SEHRA, H., ALMEIDA-KING, J., LOVELAND, J., TREVANION, S., JONES, M., QUAIL, M., WILLEY, D., HUNT, A., BURTON, J., SIMS, S., MCLAY, K., PLUMB, B., DAVIS, J., CLEE, C., OLIVER, K., CLARK, R., RIDDLE, C., ELLIOT, D., THREADGOLD, G., HARDEN, G., WARE, D., BEGUM, S., MORTIMORE, B., KERRY, G., HEATH, P., PHILLIMORE, B., TRACEY, A., CORBY, N., DUNN, M., JOHNSON, C., WOOD, J., CLARK, S., PELAN, S., GRIFFITHS, G., SMITH, M., GLITHERO, R., HOWDEN, P., BARKER, N., LLOYD, C., STEVENS, C., HARLEY, J., HOLT, K., PANAGIOTIDIS, G., LOVELL, J., BEASLEY, H., HENDERSON, C., GORDON, D., AUGER, K., WRIGHT, D., COLLINS, J., RAISEN, C., DYER, L., LEUNG, K., ROBERTSON, L., AMBRIDGE, K., LEONGAMORNLERT, D., MCGUIRE, S., GILDERTHORP, R., GRIFFITHS, C., MANTHRAVADI, D., NICHOL, S., BARKER, G., et al. 2013. The zebrafish reference genome sequence and its relationship to the human genome. *Nature,* 496**,** 498-503.

HUNG, V., UDESHI, N. D., LAM, S. S., LOH, K. H., COX, K. J., PEDRAM, K., CARR, S. A. & TING, A. Y. 2016. Spatially resolved proteomic mapping in living cells with the engineered peroxidase APEX2. *Nat Protoc,* 11**,** 456-75.

IRRCHER, I., ALEYASIN, H., SEIFERT, E. L., HEWITT, S. J., CHHABRA, S., PHILLIPS, M., LUTZ, A. K., ROUSSEAUX, M. W., BEVILACQUA, L., JAHANI-ASL, A., CALLAGHAN, S., MACLAURIN, J. G., WINKLHOFER, K. F., RIZZU, P., RIPPSTEIN, P., KIM, R. H., CHEN, C. X., FON, E. A., SLACK, R. S., HARPER, M. E., MCBRIDE, H. M., MAK, T. W. & PARK, D. S. 2010. Loss of the Parkinson's disease-linked gene DJ-1 perturbs mitochondrial dynamics. *Hum Mol Genet,* 19**,** 3734-46.

JIMENEZ-BLASCO, D., SANTOFIMIA-CASTANO, P., GONZALEZ, A., ALMEIDA, A. & BOLANOS, J. P. 2015. Astrocyte NMDA receptors' activity sustains neuronal survival through a Cdk5-Nrf2 pathway. *Cell Death Differ,* 22**,** 1877-89.

JOHNSON, W. M., GOLCZAK, M., CHOE, K., CURRAN, P. L., MILLER, O. G., YAO, C., WANG, W., LIN, J., MILKOVIC, N. M., RAY, A., RAVINDRANATH, V., ZHU, X., WILSON, M. A., WILSON-DELFOSSE, A. L., CHEN, S. G. & MIEYAL, J. J. 2016. Regulation of DJ-1 by Glutaredoxin 1 in Vivo: Implications for Parkinson's Disease. *Biochemistry,* 55**,** 4519-32.

JUNN, E., JANG, W. H., ZHAO, X., JEONG, B. S. & MOURADIAN, M. M. 2009. Mitochondrial localization of DJ-1 leads to enhanced neuroprotection. *J Neurosci Res,* 87**,** 123-9.

KIM, J. H., LEE, S. R., LI, L. H., PARK, H. J., PARK, J. H., LEE, K. Y., KIM, M. K., SHIN, B. A. & CHOI, S. Y. 2011. High cleavage efficiency of a 2A peptide derived from porcine teschovirus-1 in human cell lines, zebrafish and mice. *PLoS One,* 6**,** e18556.

KIM, J. M., CHA, S. H., CHOI, Y. R., JOU, I., JOE, E. H. & PARK, S. M. 2016. DJ-1 deficiency impairs glutamate uptake into astrocytes via the regulation of flotillin-1 and caveolin-1 expression. *Sci Rep,* 6**,** 28823.

KREBIEHL, G., RUCKERBAUER, S., BURBULLA, L. F., KIEPER, N., MAURER, B., WAAK, J., WOLBURG, H., GIZATULLINA, Z., GELLERICH, F. N., WOITALLA, D., RIESS, O., KAHLE, P. J., PROIKAS-CEZANNE, T. & KRUGER, R. 2010. Reduced basal autophagy and impaired mitochondrial dynamics due to loss of Parkinson's disease-associated protein DJ-1. *PLoS One,* 5**,** e9367.

KUMARAN, R., KINGSBURY, A., COULTER, I., LASHLEY, T., WILLIAMS, D., DE SILVA, R., MANN, D., REVESZ, T., LEES, A. & BANDOPADHYAY, R. 2007. DJ-1 (PARK7) is associated with 3R and 4R tau neuronal and glial inclusions in neurodegenerative disorders. *Neurobiol Dis,* 28**,** 122-32.

LAM, S. S., MARTELL, J. D., KAMER, K. J., DEERINCK, T. J., ELLISMAN, M. H., MOOTHA, V. K. & TING, A. Y. 2015. Directed evolution of APEX2 for electron microscopy and proximity labeling. *Nat Methods,* 12**,** 51-4.

LIU, C. 2013. Strategies for designing transgenic DNA constructs. *Methods Mol Biol,* 1027**,** 183-201.

LIU, Y. & ZHU, X. 2017. Endoplasmic reticulum-mitochondria tethering in neurodegenerative diseases. *Transl Neurodegener,* 6**,** 21.

LUO, C., RAJPUT, A. H., AKHTAR, S. & RAJPUT, A. 2007. Alpha-synuclein and tyrosine hydroxylase expression in acute rotenone toxicity. *Int J Mol Med,* 19**,** 517-21.

MAILLOUX, R. J., MCBRIDE, S. L. & HARPER, M. E. 2013. Unearthing the secrets of mitochondrial ROS and glutathione in bioenergetics. *Trends Biochem Sci,* 38**,** 592-602.

MAITA, C., MAITA, H., IGUCHI-ARIGA, S. M. & ARIGA, H. 2013. Monomer DJ-1 and its N-terminal sequence are necessary for mitochondrial localization of DJ-1 mutants. *PLoS One,* 8**,** e54087.

MARELLA, M., SEO, B. B., YAGI, T. & MATSUNO-YAGI, A. 2009. Parkinson's disease and mitochondrial complex I: a perspective on the Ndi1 therapy. *J Bioenerg Biomembr,* 41**,** 493-7.

MARTELL, J. D., DEERINCK, T. J., LAM, S. S., ELLISMAN, M. H. & TING, A. Y. 2017. Electron microscopy using the genetically encoded APEX2 tag in cultured mammalian cells. *Nat Protoc,* 12**,** 1792-1816.

MCCOY, M. K. & COOKSON, M. R. 2011. DJ-1 regulation of mitochondrial function and autophagy through oxidative stress. *Autophagy,* 7**,** 531-2.

MILLER, I. N. & CRONIN-GOLOMB, A. 2010. Gender differences in Parkinson's disease: clinical characteristics and cognition. *Mov Disord,* 25**,** 2695-703.

MOSCOVITZ, O., BEN-NISSAN, G., FAINER, I., POLLACK, D., MIZRACHI, L. & SHARON, M. 2015. The Parkinson's-associated protein DJ-1 regulates the 20S proteasome. *Nature Communications,* 6**,** 6609.

MOURADIAN, M. M. 2002. Recent advances in the genetics and pathogenesis of Parkinson disease. *Neurology,* 58**,** 179-85.

MULLETT, S. J. & HINKLE, D. A. 2009. DJ-1 knock-down in astrocytes impairs astrocyte-mediated neuroprotection against rotenone. *Neurobiol Dis,* 33**,** 28-36.

MURPHY, M. P. 2009. How mitochondria produce reactive oxygen species. *Biochem J,* 417**,** 1-13.

NAGAKUBO, D., TAIRA, T., KITAURA, H., IKEDA, M., TAMAI, K., IGUCHI-ARIGA, S. M. & ARIGA, H. 1997. DJ-1, a novel oncogene which transforms mouse NIH3T3 cells in cooperation with ras. *Biochem Biophys Res Commun,* 231**,** 509-13.

NATALE, M., BONINO, D., CONSOLI, P., ALBERIO, T., RAVID, R. G., FASANO, M. & BUCCI, E. M. 2010. A meta-analysis of two-dimensional electrophoresis pattern of the Parkinson's disease-related protein DJ-1. *Bioinformatics,* 26**,** 946-52.

NEUMANN, M., MULLER, V., GORNER, K., KRETZSCHMAR, H. A., HAASS, C. & KAHLE, P. J. 2004. Pathological properties of the Parkinson's disease-associated protein DJ-1 in alpha-synucleinopathies and tauopathies: relevance for multiple system atrophy and Pick's disease. *Acta Neuropathol,* 107**,** 489-96.

OH, S. E. & MOURADIAN, M. M. 2017. Regulation of Signal Transduction by DJ-1. *Adv Exp Med Biol,* 1037**,** 97-131.

OTTOLINI, D., CALI, T., NEGRO, A. & BRINI, M. 2013. The Parkinson disease-related protein DJ-1 counteracts mitochondrial impairment induced by the tumour suppressor protein p53 by enhancing endoplasmic reticulum-mitochondria tethering. *Hum Mol Genet,* 22**,** 2152-68.

PAILLUSSON, S., STOICA, R., GOMEZ-SUAGA, P., LAU, D. H. W., MUELLER, S., MILLER, T. & MILLER, C. C. J. 2016. There's Something Wrong with my MAM; the ER-Mitochondria Axis and Neurodegenerative Diseases. *Trends Neurosci,* 39**,** 146-157.

PARK, S. J., LEE, J. H., KIM, H. Y., CHOI, Y. H., PARK, J. S., SUH, Y. H., PARK, S. M., JOE, E. H. & JOU, I. 2012. Astrocytes, but not microglia, rapidly sense H(2)O(2)via STAT6 phosphorylation, resulting in cyclooxygenase-2 expression and prostaglandin release. *J Immunol,* 188**,** 5132-41.

PARNG, C., SENG, W. L., SEMINO, C. & MCGRATH, P. 2002. Zebrafish: a preclinical model for drug screening. *Assay Drug Dev Technol,* 1**,** 41-8.

RAHMAN-ROBLICK, R., HELLMAN, U., BECKER, S., BADER, F. G., AUER, G., WIMAN, K. G. & ROBLICK, U. J. 2008. Proteomic identification of p53-dependent protein phosphorylation. *Oncogene,* 27**,** 4854-9.

RANINGA, P. V., DI TRAPANI, G. & TONISSEN, K. F. 2017. The Multifaceted Roles of DJ-1 as an Antioxidant. *Adv Exp Med Biol,* 1037**,** 67-87.

REPICI, M., STRAATMAN, K. R., BALDUCCIO, N., ENGUITA, F. J., OUTEIRO, T. F. & GIORGINI, F. 2013. Parkinson's disease-associated mutations in DJ-1 modulate its dimerization in living cells. *J Mol Med (Berl),* 91**,** 599-611.

REYNOLDS, E. S. 1963. The use of lead citrate at high pH as an electron-opaque stain in electron microscopy. *J Cell Biol,* 17**,** 208-12.

RICHARME, G., MIHOUB, M., DAIROU, J., BUI, L. C., LEGER, T. & LAMOURI, A. 2015. Parkinsonism-associated protein DJ-1/Park7 is a major protein deglycase that repairs methylglyoxal- and glyoxal-glycated cysteine, arginine, and lysine residues. *J Biol Chem,* 290**,** 1885-97.

RINK, E. & WULLIMANN, M. F. 2004. Connections of the ventral telencephalon (subpallium) in the zebrafish (Danio rerio). *Brain Res,* 1011**,** 206-20.

SAEED, U., RAY, A., VALLI, R. K., KUMAR, A. M. & RAVINDRANATH, V. 2010. DJ-1 loss by glutaredoxin but not glutathione depletion triggers Daxx translocation and cell death. *Antioxid Redox Signal,* 13**,** 127-44.

SALIM, S. 2017. Oxidative Stress and the Central Nervous System. *J Pharmacol Exp Ther,* 360**,** 201-205.

SANTORIELLO, C. & ZON, L. I. 2012. Hooked! Modeling human disease in zebrafish. *J Clin Invest,* 122**,** 2337-43.

SCHAPIRA, A. H., MANN, V. M., COOPER, J. M., DEXTER, D., DANIEL, S. E., JENNER, P., CLARK, J. B. & MARSDEN, C. D. 1990. Anatomic and disease specificity of NADH CoQ1 reductase (complex I) deficiency in Parkinson's disease. *J Neurochem,* 55**,** 2142-5.

SHENDELMAN, S., JONASON, A., MARTINAT, C., LEETE, T. & ABELIOVICH, A. 2004. DJ-1 is a redox-dependent molecular chaperone that inhibits alpha-synuclein aggregate formation. *PLoS Biol,* 2**,** e362.

SHINBO, Y., NIKI, T., TAIRA, T., OOE, H., TAKAHASHI-NIKI, K., MAITA, C., SEINO, C., IGUCHI-ARIGA, S. M. & ARIGA, H. 2006. Proper SUMO-1 conjugation is essential to DJ-1 to exert its full activities. *Cell Death Differ,* 13**,** 96-108.

SON, O. L., KIM, H. T., JI, M. H., YOO, K. W., RHEE, M. & KIM, C. H. 2003. Cloning and expression analysis of a Parkinson's disease gene, uch-L1, and its promoter in zebrafish. *Biochem Biophys Res Commun,* 312**,** 601-7.

SURMEIER, D. J., OBESO, J. A. & HALLIDAY, G. M. 2017. Selective neuronal vulnerability in Parkinson disease. *Nat Rev Neurosci,* 18**,** 101-113.

TAKAHASHI, K., TAIRA, T., NIKI, T., SEINO, C., IGUCHI-ARIGA, S. M. & ARIGA, H. 2001. DJ-1 positively regulates the androgen receptor by impairing the binding of PIASx alpha to the receptor. *J Biol Chem,* 276**,** 37556-63.

THERMES, V., GRABHER, C., RISTORATORE, F., BOURRAT, F., CHOULIKA, A., WITTBRODT, J. & JOLY, J. S. 2002. I-SceI meganuclease mediates highly efficient transgenesis in fish. *Mech Dev,* 118**,** 91-8.

TROPEPE, V. & SIVE, H. L. 2003. Can zebrafish be used as a model to study the neurodevelopmental causes of autism? *Genes Brain Behav,* 2**,** 268-81.

TWELVES, D., PERKINS, K. S. & COUNSELL, C. 2003. Systematic review of incidence studies of Parkinson's disease. *Mov Disord,* 18**,** 19-31.

VAN HORSSEN, J., DREXHAGE, J. A., FLOR, T., GERRITSEN, W., VAN DER VALK, P. & DE VRIES, H. E. 2010. Nrf2 and DJ1 are consistently upregulated in inflammatory multiple sclerosis lesions. *Free Radic Biol Med,* 49**,** 1283-9.

WAAK, J., WEBER, S. S., WALDENMAIER, A., GORNER, K., ALUNNI-FABBRONI, M., SCHELL, H., VOGT-WEISENHORN, D., PHAM, T. T., REUMERS, V., BAEKELANDT, V., WURST, W. & KAHLE, P. J. 2009. Regulation of astrocyte inflammatory responses by the Parkinson's disease-associated gene DJ-1. *FASEB J,* 23**,** 2478-89.

WAGENFELD, A., YEUNG, C. H., STRUPAT, K. & COOPER, T. G. 1998. Shedding of a rat epididymal sperm protein associated with infertility induced by ornidazole and alpha-chlorohydrin. *Biol Reprod,* 58**,** 1257-65.

WILSON, M. A., COLLINS, J. L., HOD, Y., RINGE, D. & PETSKO, G. A. 2003. The 1.1-A resolution crystal structure of DJ-1, the protein mutated in autosomal recessive early onset Parkinson's disease. *Proc Natl Acad Sci U S A,* 100**,** 9256-61.

XI, Y., NOBLE, S. & EKKER, M. 2011. Modeling neurodegeneration in zebrafish. *Curr Neurol Neurosci Rep,* 11**,** 274-82.

ZAGOURA, D., CANOVAS-JORDA, D., PISTOLLATO, F., BREMER-HOFFMANN, S. & BAL-PRICE, A. 2017. Evaluation of the rotenone-induced activation of the Nrf2 pathway in a neuronal model derived from human induced pluripotent stem cells. *Neurochem Int,* 106**,** 62-73.

ZENG, X. S., GENG, W. S. & JIA, J. J. 2018. Neurotoxin-Induced Animal Models of Parkinson Disease: Pathogenic Mechanism and Assessment. *ASN Neuro,* 10**,** 1759091418777438.

ZHANG, L., SHIMOJI, M., THOMAS, B., MOORE, D. J., YU, S. W., MARUPUDI, N. I., TORP, R., TORGNER, I. A., OTTERSEN, O. P., DAWSON, T. M. & DAWSON, V. L. 2005. Mitochondrial localization of the Parkinson's disease related protein DJ-1: implications for pathogenesis. *Hum Mol Genet,* 14**,** 2063-73.

ZHANG, Y., LI, X. R., ZHAO, L., DUAN, G. L., XIAO, L. & CHEN, H. P. 2018. DJ-1 preserving mitochondrial complex I activity plays a critical role in resveratrol-mediated cardioprotection against hypoxia/reoxygenation-induced oxidative stress. *Biomed Pharmacother,* 98**,** 545-552.